ON THE HISTORY OF EXPANSION AND MATTER-ENERGY CONTENT OF THE UNIVERSE

by

Ali Kazım Çamlıbel

B.S., Physics, Boğaziçi University, 2005

M.S., Physics, Boğaziçi University, 2009

Submitted to the Institute for Graduate Studies in
Science and Engineering in partial fulfillment of
the requirements for the degree of
Doctor of Philosophy

Graduate Program in Physics

Boğaziçi University

2016

ACKNOWLEDGEMENTS

First of all, I wish to express my gratitude to my supervisor, İbrahim Semiz, whose wisdom and invaluable guidance made this work possible. I can not thank enough for the time and effort that he invested in my studies.

I would like to thank people at the Physics Department, especially Koray Düztaş for valuable discussions and Serhat Işţın, Cemile Ezer and Bora Işıldak for their true friendship during the past six years.

I would like to express my sincere thanks to Nihal Ercan and the people at the Astrophysics Laboratory for the welcoming environment during the past three months.

I thank my dear family for being there for me whole my life with their unconditional love and support.

And I thank my beloved wife, Burcu; her love gave me power to carry on and being around her was the true inspiration for my studies.

ABSTRACT

ON THE HISTORY OF EXPANSION AND MATTER-ENERGY CONTENT OF THE UNIVERSE

The aim of this dissertation is to explore the vast phenomenological area between the cosmological observations and the theoretical approaches. We are specifically focusing on type Ia supernova data and what they tell us in the manner of expansion history of the universe. In this regard, we start by introducing the current status of cosmological observations including cosmic microwave background radiation, galaxy redshift surveys, supernova missions, etc. We briefly summarise the standard approaches of data analysis and cosmological parameter estimation. Then, we introduce our own approach, where we use only the cosmological principle and the assumption that gravitation is governed by a metric theory and try to reconstruct the expansion history from supernova data. We find that the acceleration history of the universe cannot be reliably determined in this approach due to the irregularity and parametrisation-dependence of the results. Therefore we add gamma ray bursts to our analysis and in doing so we become able to estimate the redshift of transition to cosmic acceleration and additionally –assuming Einstein gravity– put a lower limit to dark energy density.

Next we introduce three ideas on the expansion characteristics of the universe and examine if they are compatible with observations. First we explore the idea of massive photons and how it would affect our observations. Secondly, we present an ansatz for the deceleration parameter for a model in which dark matter decays into dark energy, inspired by the theory of relativistic cosmic fluids. Lastly, inspired by the web-like large scale structure we introduce an inhomogeneous equation of state from fluid dynamics and examine its cosmological implications.

ÖZET

EVRENİN GENİŞLEME TARİHİNE VE MADDE-ENERJİ İÇERİĞİNE DAİR

Bu tezdeki amacımızı, kozmolojik gözlemlerle, onları açıklamak için geliştirilen teorik yaklaşımlar arasındaki geniş alanın araştırılması olarak ifade etmek mümkün. Bu amaç doğrultusunda tip Ia süpernova verisine ve bu verinin bize evrenin genişleme geçmişine dair ne anlattığına odaklanmaktayız. Bu bağlamda, öncelikle kozmik ardalan ışıması, gökada kızılakayma araştırmaları, süpernova gözlemleri gibi kozmolojik verilerin güncel durumlarından bahsediyoruz. Veri analizi ve kozmolojik parametrelerin belirlenmesinin standart yollarını kısaca anlatıyoruz. Ardından sadece kozmolojik ilke ve genelçekimin metrik teori olduğu kabullerini içeren kendi yaklaşımımızı sunuyoruz. Bu yaklaşım sonucu evrenin genişleme geçmişinin, sonuçların düzensizliği ve parametrelere bağımlılığı sebebiyle güvenilir bir şekilde belirlenemediğini gösteriyoruz. Bu sebeple analizimize gama ışını patlamalarını ekliyoruz ve böylelikle kozmik hızlanmaya geçiş kızılakaymasını belirliyoruz. Ayrıca –Einstein genelçekimi kabulüyle– karanlık enerji yoğunluğuna bir alt limit getirebiliyoruz.

Sonrasında ortaya evrenin genişleme özellikleri üzerine üç adet fikir sunuyoruz ve bunların gözlemlerle uyumlu olup olmadıklarına bakıyoruz. İlk olarak kütleli fotonları ve bunların gözlemleri nasıl etkileyebileceğini inceliyoruz. İkinci olarak, relativistik kozmik akışkanların teorisinden yola çıkarak, karanlık maddenin karanlık enerjiye bozunduğu bir modelde ivme parametresi için bir önerme sunuyoruz. Son olaraksa, evrenin örümcek ağına benzer büyük ölçekli yapısından esinlenerek akışkanlar mekaniği kaynaklı, türdeş olmayan bir hal denkleminin kozmolojik sonuçlarını inceliyoruz.

TABLE OF CONTENTS

ACKNOWLEDGEMENTS iii
ABSTRACT iv
ÖZET v
LIST OF FIGURES vii
LIST OF TABLES xii
LIST OF SYMBOLS xiii
LIST OF ACRONYMS/ABBREVIATIONS xv
1. INTRODUCTION 1
2. OBSERVATIONAL COSMOLOGY: THE STATE OF AFFAIRS 9
2.1. Distance measures in homogeneous and isotropic background 9
2.2. Measuring the inhomogeneities in the universe 10
2.2.1. CMB anisotropies 10
2.2.2. Galaxy-redshift surveys and Lyman-α forest 12
3. EXPANSION OF SPACE: WHAT CAN WE GET FROM OBSERVATIONS? 16
3.1. Mathematical Framework and Motivation 16
3.2. Fitting the luminosity distance function 20
3.2.1. Alternative variables 20
3.2.2. The candidate families and the fits 21
3.3. Determination of the expansion history of the universe 29
3.3.1. More on the procedure 29
3.3.2. Determination of time derivatives of the scale function 30
3.3.3. Is the universe accelerating *now*? 38
3.4. Inferences in GR about the content of the universe 40
4. IDEAS ON THE EXPANSION OF THE UNIVERSE 46
4.1. Modelling the expansion between two regimes 46
4.2. Massive photons and modifications on observations 49
4.3. Foam-like structure and its cosmological implications 50
5. CONCLUSION 55
REFERENCES 58

LIST OF FIGURES

Figure 1.1. Plots showing the sensitivities of the peaks in CMB power spectrum to various parameters of ΛCDM model. In each panel the varied quantity is indicated on the color legend. $\Omega_{\rm tot}$ is kept constant for all panels except the upper left one which is obtained for fixed Ω_Λ. 7

Figure 2.1. Harmonic peaks from the analysis of CMB anisotropy data (red circles); the height of each peak corresponds to the *power* of each mode, hence a power spectrum. The fitted curve is the six parameter spatially flat ΛCDM model. 12

Figure 2.2. Degeneracy between $\Omega_{\rm M}$ and H_0 as illustrated in [16]. 13

Figure 2.3. A recent BAO Hubble diagram. Each survey measures $D_{\rm V}$ around a pivoting redshift value, so it is possible to plot $D_{\rm V}$ vs z diagram. Adapted from [17]. 14

Figure 2.4. Hubble parameter estimation through galaxy power spectra (blue, green, black) requires additional information on $d_{\rm A}(z)$. Lyman-α data (red) however can give $H(z)$ by themselves. Results are consistent with an early deceleration. Adapted from [18]. 15

Figure 3.1. Parameter space for a ΛCDM universe with constraints from various observations. 17

Figure 3.2. Relation betweeen the redshift variables y_0-y_5 and the scale factor. Note that y_3 is not monotonic with a. 21

Figure 3.3. Union 2.1 data (in terms of luminosity distance and standard redshift $z \equiv y_0$); the N=2 to 7 fits for the first family, i.e. simple polynomials; the fits for the MD (black) and ΛCDM (red) models, and the one-sigma confidence-levels of the best-fitting member (N=4) of the family F1. The inset shows the right end, magnified. Note the strange behaviour of F17. 24

Figure 3.4. Union 2.1 data (in terms of luminosity distance and redshift $z \equiv y_0$); and best fits for each function family listed in Table 3.2. The one-sigma confidence-levels are not shown to not clutter up the figure; they are similar to those in Figure 3.3. 25

Figure 3.5. Same as in Figure 3.4 but with the redshift variable y_1. 25

Figure 3.6. Same as in Figure 3.4 but with the redshift variable y_2. 26

Figure 3.7. Same as in Figure 3.4 but with the redshift variable y_4. 26

Figure 3.8. Same as in Figure 3.4 but with the redshift variable y_5. 27

Figure 3.9. Same as in Figure 3.4 but with the redshift variable $y_6 = u = 1 + z$. 27

Figure 3.10. χ^2_ν values in Table 3.2, illustrated as a 3D bar chart for different function families and redshift variables. 28

Figure 3.11. The $a(t)$ functions, computed by numerical integration of Eq. 3.3 and subsequent numerical inversion to find $z(t)$ (or similar analysis with one of the redshift variables y_i), using the fits found for $d_L(y_i)$ to the Union 2.1 data. The columns represents analyses with y_0, y_1, y_2, y_4, y_5 and u, respectively, and rows are for candidate families F1-F8. In each plot, the horizontal axis is t, ticked at 1 Gyr intervals, and the vertical axis is $a(t)$, normalized to 1 at the present epoch shown at the right end of each plot. For curvature, the same color-coding is used as in Figure 3.12, but the curves for different curvatures practically overlap in this figure. 31

Figure 3.12. The $\dot{a}(z)$ functions, computed analytically for the Union 2.1 data by Eq. 3.13 or its analogs for the different redshift variables y_i. The columns and rows have the same meaning as in the previous figure. Blue, red and black curves represent open, closed and flat spaces respectively, with the range $-\kappa_0 \leq \kappa \leq \kappa_0$. For comparison purposes, the horizontal axes are transformed to be $z = y_0$, ticked with intervals $\Delta z = 0.2$, and $\dot{a}(0)$ is normalized to 1 in $(H_0 a_0)$ units. 32

Figure 3.13. All $\ddot{a}(z)$ functions, computed analytically to the Union 2.1 data by Eq. 3.14 or its analogs for the different redshift variables y_i. The columns, rows and colors have the same meaning as in the previous figure. For comparison purposes, the horizontal axes are transformed to be $z = y_0$, ticked with intervals $\Delta z = 0.2$, and the vertical axes are in arbitrary units. 33

Figure 3.14. The Union 2.1 supernova data, shown in blue, the GRB data [13], shown in red, and the quasar [14] data shown in black, together. . 34

Figure 3.15. The $\ddot{a}(z)$ functions, computed analytically by Eq. 3.14 or its analogs for the different redshift variables y_i. The rows, columns and color coding have the same meaning as in Figures 3.11-3.13, fitted to the Union 2.1 and GRB data. For comparison purposes, the horizontal axes are transformed to be $z = y_0$, ticked with intervals $\Delta z = 0.2$,and the vertical axes are in arbitrary units. 35

Figure 3.16. χ^2_ν values in Table 3.3, illustrated as a 3D bar chart for different function families and redshift variables. 36

Figure 3.17. The average of the fifteen "natural" $\ddot{a}(z)$ functions from Figure 3.15, namely those in columns one, five and six, and rows two, four, six, seven and eight, extended to negative z, i.e. to the future. The color coding has the same meaning as in Figures 3.11-3.13. The horizontal axis shows $z = y_0$, ticked with intervals $\Delta z = 0.1$, and the vertical axis is in arbitrary units. 37

Figure 3.18. Acceleration history for the whole range including GRB data, plotted for function family F7 and redshift variable $y5$. 39

Figure 3.19. The density of the universe as function of $u = z + 1$, as calculated using the redshift variable $y5$ and fit family F7, assuming Einstein gravity. The color-coding is the same as used in Figure 3.12. Note the intersection around $z \approx 1.5$. The dashed curve shows matter density, passing through the intersection point. 41

Figure 3.20. The average $w(z)$, in the framework of Einstein gravity, found from the fifteen functions we used in Figure 3.17, extended to negative z, i.e. to the future. The color coding has the same meaning as in Figures 3.11-3.13. 44

Figure 4.1. Evolution of deceleration parameter between radiation and matter dominated eras. Horizontal axis shows $1/\theta = mc^2/k_BT$. 47

Figure 4.2. Evolution of deceleration parameter between matter and Λ dominated eras. 48

Figure 4.3. Massive photon cosmology (blue) with ΛCDM (red) and matter dominated model (black) compared to Union 2.1 data. 51

LIST OF TABLES

Table 3.1. The 8 different families used in fits. y can be any one of the redshift parameters described in Sect. 3.2.1, $P_N(y)$ is the N^{th} order polynomial with zero constant term (except when using $y_6 = u$, see Sect. 3.2.2), $u(y)$ is $(1+z)$ expressed in terms of y, Pade(y, M, N) is the Padé approximant in variable y and orders M & N; and c & d are constants. 23

Table 3.2. The best fits for the Union 2.1 SNe Ia data. Each cell displays the internal label(s) of the best-fitting member of the row's family for the column's redshift variable, and the fit's $\chi^2_\nu \equiv \chi^2/\text{d.o.f}$ value. Note that $\chi^2_\nu = 0.9340$ for ΛCDM (the variable is $y_0 = z$). 28

Table 3.3. The best fits for the Union 2.1 SNe Ia + GRB data. Each cell displays the internal label of the best-fitting member of the family for that row and the $\chi^2_\nu \equiv \chi^2/\text{d.o.f}$ value associated with the redshift variable for that column 36

Table 3.4. z_* and $\Omega_{0m,\max}$ with their estimated errors calculated for 15 different $d_L(z)$ functions and assuming Einstein gravity. 43

LIST OF SYMBOLS

$a(t), a(z)$	Scale factor of the universe
A	Normalised scale factor
c	Speed of light
d_A	Angular diameter distance
d_L	Luminosity distance
D	Photon count distance
D_V	Volume distance
G	Gravitational constant
h	Planck's constant
H	Hubble parameter
I	Intensity
k	Curvature parameter
k_B	Boltzmann constant
K	Kinetic energy
L	Luminosity
N	Amplitude of primordial perturbations
p	Pressure
q	Deceleration parameter
V	Volume
w	Equation of state parameter
z	Redshift
γ	Lorentz factor
δ	Density field
κ	Curvature function
λ	Wavelength
Λ	Cosmological constant
ξ	Correlation function

ρ	Energy density
σ	Surface tension
σ_s	Surface mass density
τ	Optical depth to last scattering surface
Ω	Energy density fraction

LIST OF ACRONYMS/ABBREVIATIONS

2dF	Two degree Field
3D	Three Dimensional
6dF	Six degree Field
BAO	Baryon Acoustic Oscillations
BOSS	Baryon Oscillation Spectroscopic Survey
CDM	Cold Dark Matter
CfA	Center for Astrophysics
CMB	Cosmic Microwave Background
COBE	Cosmic Background Explorer
COMB	Compact Embedded Object Simulations
COSMOMC	Cosmological Monte Carlo
DE	Dark Energy
DES	Dark Energy Survey
DM	Dark Matter
EoS	Equation of State
ESA	European Space Agency
FRW	Friedman-Robertson-Walker
GR	General Relativity
GRB	Gamma Ray Burst
LIGO	Laser Interferometer Gravitational-Wave Observatory
MD	Matter Dominated
WMAP	Wilkinson Microwave Anisotropy Probe
SDSS	Sloan Digital Sky Survey
SN	Supernova
SN Ia	Supernova type Ia

1. INTRODUCTION

Observational cosmology, a relatively young research area, is established on extensive data from very different types of astrophysical sources and relies on diverse data mining and numerical analysis methods; yet the whole field can be roughly summarised as the search for an answer to two questions:

- How is the expansion of the space evolving in time?
- How is the matter distributed in space?

These questions can be reformulated, given in more detail or quantified but adding a third one to this list is a difficult job. For example, popular questions on the nature of *dark energy* or *dark matter* will involve too many assumptions at first hand and even tough some answers may be there in the data, they will manifest themselves in the form of the answers to the above.

The first of these questions, the one on the expansion of the space, can be traced back to observations of Edwin Hubble [1], obviously. Fundamentals of the query have not changed much since then; find a distant object for which you can estimate a distance indicator independently (i.e. a *standard candle*) and along with its redshift you get a glimpse on the expansion characteristics. These objects are then test particles acting as flags on the spacetime fabric governed by a metric theory. Within the framework of a homogeneous and isotropic universe these are the data that will give the *scale function* for the universe; the function that will uniquely give the expansion of space as a function of time. The only free parameter will be the curvature of space, which must be constrained through other data sets or theories. This part of the analysis is often dubbed as the *kinematical approach* [2] or *cosmography* [3]: doing cosmology without any emphasis on matter-energy content and gravity theory. A further step may be to incorporate a gravity theory e.g. Einstein's general relativity and therein speculate on matter-energy content.

There might be a variety of astrophysical objects, which can be identified as standard candles in principle, yet the most useful ones today are type Ia supernova (SNe Ia) events; their observations consist of measurements of their redshifts z and their distance moduli μ, a logarithmic scale for brightness. The distance moduli can be converted to luminosity distances according to

$$d_L(z) = 3.26 \times 10^{0.2\mu+1} \text{ ly} \tag{1.1}$$

where the standard definition of luminosity distance is

$$d_L^2 \equiv \frac{L}{4\pi I} \tag{1.2}$$

the distance an object of luminosity L would be judged to be in static flat space, if it produced an intensity I on Earth.

As stated before, the assumptions of homogeneity and isotropy lead to a description of the spacetime in terms of scale factor $a(t)$ and curvature parameter k only. The metric that follows from those assumptions is called Friedman-Robertson-Walker (FRW) and can be written as the line element,

$$ds^2 = -c^2dt^2 + a^2(t)\left[\frac{dr^2}{1-kr^2} + r^2(d\theta^2 + \sin^2\theta d\phi^2)\right] \tag{1.3}$$

To analyse the relation between the scale factor and the redshift we consider the propagation of light, i.e. a radial null geodesic, meaning $ds^2 = 0$, $d\theta = 0$, $d\phi = 0$. We get

$$c^2dt^2 = a^2(t)\frac{dr^2}{1-kr^2} \tag{1.4}$$

and

$$\frac{cdt}{a(t)} = \pm\frac{dr}{(1-kr^2)^{1/2}} \tag{1.5}$$

Integrating both sides we find,

$$c\int_{t_1}^{t_0}\frac{dt}{a(t)} = -\int_{r_1}^{0}\frac{dr}{(1-kr^2)^{1/2}} = f(r_1) \tag{1.6}$$

for a wave crest of light propagating from $r = r_1$ to the origin in the time interval from t_1 to t_0; where $f(r_1)$ depends on curvature parameter k. Assuming that another wave crest is generated at time $t = t_1 + dt_1$ at $r = r_1$ and it is observed at $t = t_0 + dt_0$ at the origin, our equations become

$$c\int_{t_1+dt_1}^{t_0+dt_0}\frac{dt}{a(t)} = -\int_{r_1}^{0}\frac{dr}{(1-kr^2)^{1/2}} = f(r_1) \tag{1.7}$$

from which we can conclude that

$$\int_{t_1}^{t_0}\frac{dt}{a} = \int_{t_1+dt_1}^{t_0+dt_0}\frac{dt}{a} \tag{1.8}$$

or simply,

$$\frac{dt_0}{a(t_0)} = \frac{dt_1}{a(t_1)} \tag{1.9}$$

So we can easily define the cosmological redshift z as a fraction of time intervals or basically frequencies;

$$1 + z = \frac{dt_0}{dt_1} = \frac{a(t_0)}{a(t_1)} \tag{1.10}$$

Now let's get back to definition of the luminosity distance (1.2). For a static and flat geometry d_L would be equal to the proper distance. In our context this is

$$d_L = a(t_0)r_1 \tag{1.11}$$

where r_1 is the coordinate of emission. But in an expanding universe the luminosity

is reduced by a factor of $(1+z)^2$ since it is energy radiated per unit time and both energy and inverse time interval are redshifted by $(1+z)$. So,

$$d_L^2 = a^2(t_0) r_1^2 (1+z)^2 \tag{1.12}$$

where r_1 can be related to the emission time by (1.6), i.e. by the inverse of the function $f(r)$. The $f(r)$ functions for the three available k values are, from Equation 1.6,

$$f(r_1) = c\int_{t_1}^{t_0} \frac{dt}{a} = \begin{cases} \sin^{-1}(r_1), & k=1 \\ r_1, & k=0 \\ \sinh^{-1}(r_1), & k=-1 \end{cases} \tag{1.13}$$

Since we measure z, not t, we need to replace dt with dz. To that end, we take the derivative of (1.10);

$$\frac{dz}{dt} = -(1+z)H(z) \tag{1.14}$$

So

$$c\int_{t_1}^{t_0} \frac{dt}{a(t)} = -c\int_{z}^{0} \frac{dz'}{a(z')(1+z')H(z')} = \frac{c}{a(t_0)}\int_0^z \frac{dz'}{H(z')} = f(r_1) \tag{1.15}$$

and

$$r_1 = f^{-1}\left(\frac{c\int_0^z \frac{dz'}{H(z')}}{a(t_0)}\right) \tag{1.16}$$

Finally the luminosity distance from (1.12) becomes [4]

$$d_L(z) = (1+z)a_0 f^{-1}\left(\frac{c\int_0^z \frac{dz'}{H(z')}}{a_0}\right) \tag{1.17}$$

Note that these results follow from the assumption of the FRW metric, without using Einstein or alternative theory of gravity.

If one assumes a theory of gravity and determines which fluids are contributing to the content of the universe (hence constructs a *model*), it is possible to calculate the corresponding $a(t)$. Many models have been put forward, e.g. featuring fluids with different EoS's. To evaluate any such theory, or determine the best values of the theory's parameters, usually the same procedure is followed; i.e. $a(t)$ is determined from the assumptions of the theory, then $d_L(z)$ is evaluated using Eq. 1.17, and checked against the data to assess the viability of the model. The main body of this thesis, starting with chapter 3, however, introduces a different approach, where we try to find $d_L(z)$ functions that are good fits to the data and move on to construct $a(t)$ from there. We are able to do this without an emphasis on the matter-energy content of the universe or theory of gravity, apart from being a metric theory, hence cosmographically.

The research on the matter distribution, however, is different from the research on expansion, both observationally and mathematically. First of all, data come from different sources like in the form of anisotropy in the *cosmic microwave background radiation* (CMB) or in the form of galaxy surveys where one maps *large scale structures* in the sky. There are also *Lyman-α forest* surveys telling us the line-of-sight matter distribution between ourselves and a distant quasar and there are surveys mapping the dark matter distribution through *weak gravitational lensing*. Mathematically, it is necessary to introduce a deviation from homogeneity and isotropy assumptions in the form of perturbations in metric and energy-momentum tensor. A framework much more complicated obviously, this field of research has two other fundamental drawbacks in comparison with the previous one.

First of all, observables in such a survey (e.g. galaxies in a galaxy redshift survey) are not seen as tracers of general behaviour of the universe as in homogeneous cosmology, they are constituents of the structure we want to examine. As a consequence, the function we get from such data (*two-point correlation function* or its Fourier space analog, *power spectrum*) is nothing but statistics and will not give much physical information without assumptions on the matter-energy content and theory of gravity unlike the scale function we reconstruct from expansion data which has clear meaning independent of content or gravity theories. In other words physics analysis of galaxy

distribution or CMB data can not be cosmographic; dynamics must be involved. To be more specific let us point out one common misconception: It is often mentioned that the position of the first peak in the CMB anisotropy power spectrum independently gives the spatial curvature of the universe. But in fact the position of this peak is also sensitive to the introduced physical model. For example dependence on the dark energy contribution is very well illustrated in Figure 1.1 from [5]. On the upper left panel of that figure, $\Omega_{\rm tot}$ is varied while relative contributions from matter-energy components are fixed. The upper right panel shows that the first peak slightly shifts with varying dark energy contribution with fixed $\Omega_{\rm tot}$. This degeneracy between $\Omega_{\rm tot}$ and Ω_Λ is called angular diameter degeneracy. The lower left panel is the sensitivity to baryon density in fixed $\Omega_{\rm tot}$ and $\Omega_{\rm M}$ and the lower right panel is the sensitivity to matter density in fixed $\Omega_{\rm tot}$ [5]. In short, CMB anisotropy does not unequivocally tell us that the universe is flat, it can do so only for a given physical model.[1]

Apart from that data coming from the galaxy redshift surveys are in the form of angular position and redshift. To get a correlation function in three dimensions one must convert the redshift data to distances which requires a fiducial cosmology at first hand and testing cosmological models through that procedure is even considered a consistency check [6]. (Obviously this one applies to galaxy data; CMB anisotropy statistics is on a two dimensional surface already.)

For the readers who are dissatisfied with the simplification given in the beginning of this section: Yes, there are observables in the universe other than the ones that serve the aforementioned tasks in cosmology. Polarisation in CMB, if detected, will be the prominent indicator of *primordial gravitational waves* [5] (not to be confused with the astrophysical gravitational waves detected by LIGO experiment [7] during the writing of this text.). Measurement of the light nuclei abundance is still an important field of research with open questions on big bang nucleosynthesis like Li-7 problem [8]. Lastly, there are the large scale peculiar velocity measurements, a global generalisation of the

[1] By no means we intend to say that flatness of our universe is in dispute. Flat models are highly favoured by data. But when introducing a new model or especially a modification to general relativity assuming flatness beforehand can be problematic.

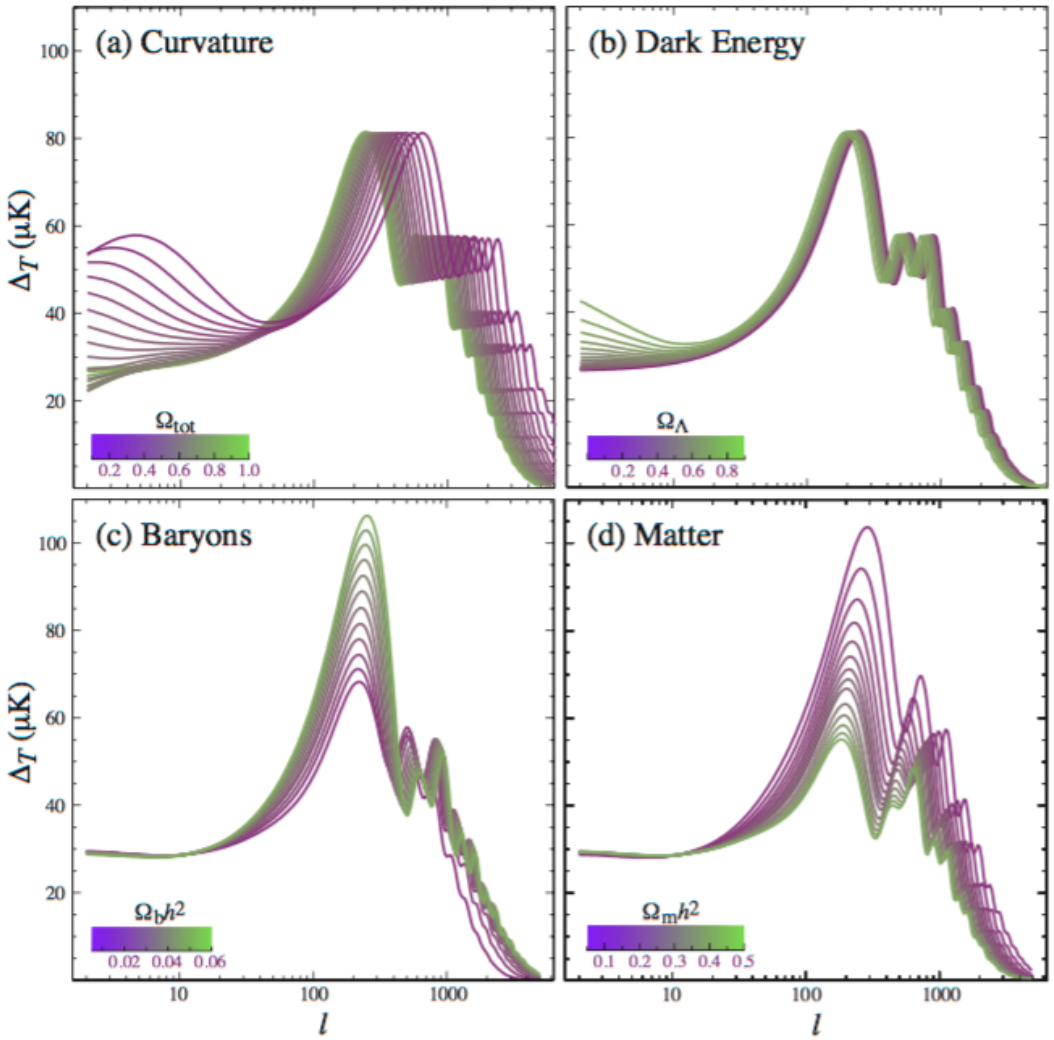

Figure 1.1. Plots showing the sensitivities of the peaks in CMB power spectrum to various parameters of ΛCDM model. In each panel the varied quantity is indicated on the color legend. Ω_{tot} is kept constant for all panels except the upper left one which is obtained for fixed Ω_Λ.

galaxy rotation curve observations [9].

In this thesis we are going to focus mostly on the expansion of the homogeneous and isotropic universe. The next chapter deals with the current state of cosmological observations and their relations to the cosmological parameters we want to constrain. Chapter 3 focuses on supernova type Ia (SN Ia) data; and on how and to what extent they give the expansion history of our universe. Our aim will be to get the most information with minimum number of assumptions, i.e. cosmographic approach outlined

above. In chapter 4 we will put forward three alternative ideas on the expanding space and see if they explain supernova data or give reasonable solutions to the cosmological constant problem.

2. OBSERVATIONAL COSMOLOGY: THE STATE OF AFFAIRS

2.1. Distance measures in homogeneous and isotropic background

At the very end of the 20^{th} century with the SNe Ia observations [10, 11] it was seen that the expansion data are not consistent with a standard cold dark matter model in which universe is dominated by matter (light and dark) on a Friedman-Robertson-Walker (FRW) framework operating under Einstein gravity theory. Two teams utilised a total number of 58 high redshift supernovae observed between the years 1992 and 1997, ranging in the redshift interval $0.18 < z < 0.83$.

Since then SN Ia observation missions went on; both from ground observatories and space telescopes. As of May 2016, the most recent and comprehensive catalog is Union 2.1 [12], with 580 SNe Ia making the cuts of reliability and in a redshift range up to $z = 1.5$. The consensus is that when the data are analysed in a FRW framework the second time derivative of the scale function is positive; hence expansion is accelerated, a feature which is inconsistent with matter domination in Einsteinian gravity. We'll come back to that problem in the following chapters.

SNe Ia are still the most profound measures of distance in cosmology. According to the *consensus model*, they originate from binary systems where matter accretes from a red giant towards a white dwarf. The energy of the incoming stream of matter results in an increase in the temperature of the white dwarf and at a scale close to the Chandrasekar mass, carbon fusion starts to take place. Because the pressure is supplied by degenerate electrons, a white dwarf cannot regulate the heat output of the fusion reactions like a main sequence star does by expanding, so fusion reactions accelerate with a great rate resulting in an explosion. The amount of carbon and oxygen that are fused can be estimated, therefore we have a fair estimation for the power output of the explosion and we can assign a distance to supernovae in relation

with their observed luminosity; definition of a standard candle. Yet throughout the years other astrophysical objects were examined if they can be used as *standardisable* candles if not standard candles already. The most popular candidates for such a job are the gamma ray bursts (GRB), the brightest electromagnetic sources in the sky coming from redshifts up to $z \sim 6$. Their standardisation process involves relating their light curve features like *lag, peak energy, variability, the minimum rise time, number of peaks* (so-called luminosity indicators) to their source luminosities [13]. Since the physical mechanisms behind GRB's are not very well known, the proposed luminosity relations remain empirical. Yet every new step in the distance ladder in astrophysics needs to be calibrated with the step below. Due to the lack of knowledge about the low-z GRB's, calibrations are made either using a cosmological model or cosmographic parameters derived from SNe data, which have large error bars and are highly scattered at high redshifts themselves. Thus the derived luminosity distances cannot be said to be model-independent.

Quasars, strong galactic nuclei sources associated with supermassive black holes from an early universe epoch around $z \sim 6$, are suggested to be standardisable [14]. Like GRB's their calibration heavily depends on cosmological model. In our analysis in the following chapter we considered to use both GRB's and quasars as part of our Hubble diagram and decided to use GRB's only on the grounds that they are spread out on a wider range of redshift and they have more reasonable error bars compared to quasars.

2.2. Measuring the inhomogeneities in the universe

2.2.1. CMB anisotropies

The Planck satellite, the successor of COBE and WMAP missions, took very high precision measurements of fluctuations in CMB temperature from 2009 to 2013 with a temperature sensitivity of $\sim 10^{-6}$. The team published their latest results in 2015 [15] two years after the satellite was deactivated. It gave the most elaborate power spectrum of temperature anisotropies yet (Figure 2.1). This is the main data that is

compared with the famous six parameter flat ΛCDM model. The actual parameter estimation is done by computer programs like CosmoMC or COMB, but as stated in [4], *neither the derivation of the formulas for temperature fluctuations nor the computer programs are physically very transparent.* Nevertheless, it is possible with considerable effort to come up with a lengthy expression that relate cosmological parameters to the power spectrum of CMB anisotropies [4, Eq. 7.2.41]. In essence, the observed power spectrum is related to two sets of parameters. The first set consists of the ones that characterise the universe after photon-baryon decoupling which are Ω_{M}, Ω_{Λ}, Ω_{K} and H_0, all introduced through the angular diameter distance d_{A} to the last scattering surface. The other set is related to the conditions in the early universe: The primordial power spectrum $P(k) \propto k^{n_s-1}$ introduces spectral index n_s, whose deviation from one quantifies the scale non-invariance of the initial perturbations. This initial spectrum is multiplied with transfer functions for different eras between inflation and decoupling and those are mainly functions of baryon density Ω_{B} and dark matter density Ω_{DM}. There are two additional overall factors, N^2, the amplitude of primordial perturbations and a reduction factor $e^{-2\tau}$ from reionization due to formation of first stars at $z \sim 10$. The parameter τ is called *optical depth to reionization surface.*

The model introduces strong degeneracies. Parameters Ω_{M}, Ω_{Λ}, Ω_{K} and H_0 are all present in d_{A}, therefore their independent determination requires additional information. The main analysis assumes a flat cosmology, therefore the dark energy density is constrained as $\Omega_{\Lambda} = 1 - \Omega_{\mathrm{M}}$. However the degeneracy between Ω_{M} and H_0 remains (Figure 2.2). The overall factor of $N^2 e^{-2\tau}$ brings about an apparent degeneracy also. Those are lifted with the use of CMB lensing data though.

The detailed results of the CMB temperature anisotropy for flat ΛCDM and neighbouring models can be found in [15]. Considering ΛCDM, they are in remarkable agreement with the other cosmological indicators and significantly improve the constraints on inflationary models.

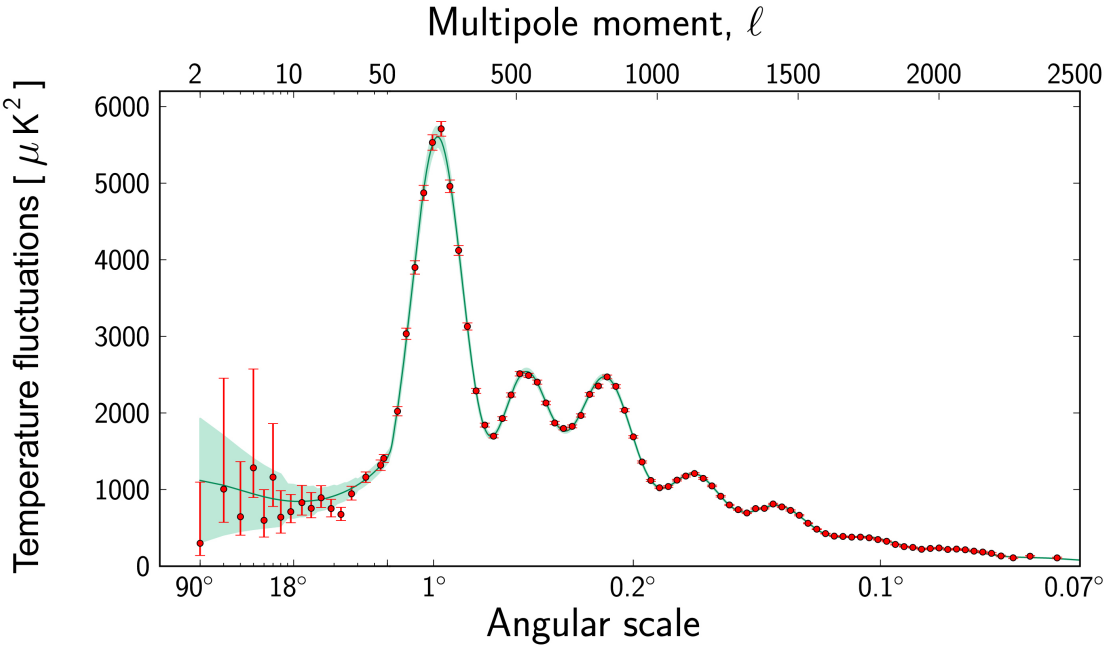

Figure 2.1. Harmonic peaks from the analysis of CMB anisotropy data (red circles); the height of each peak corresponds to the *power* of each mode, hence a power spectrum. The fitted curve is the six parameter spatially flat ΛCDM model.

2.2.2. Galaxy-redshift surveys and Lyman-α forest

The origin of galaxy redshift surveys can be traced back to 1970's, when the CfA Redshift Survey started. Despite the technological limitations of the time, researchers were able to make significant observations in the 1980's like the discovery of the Great Wall, a superstructure of galaxies. With the improvements in imaging technologies in the 1990's galaxy redshift surveys became able to aim at larger distances. The chain of important surveys began with 2dF galaxy redshift survey followed by the missions like 6dF, SDSS and WiggleZ. The most recent and comprehensive data are taken by SDSS-III, covering a field of 9376 deg^2 in the sky reporting 1,372,737 galaxy and 294,512 quasar spectra.

Galaxy redshift surveys, unlike CMB missions, operate in volume spanned by a field of view and a redshift interval. Data, acquired in redshift-angular position space

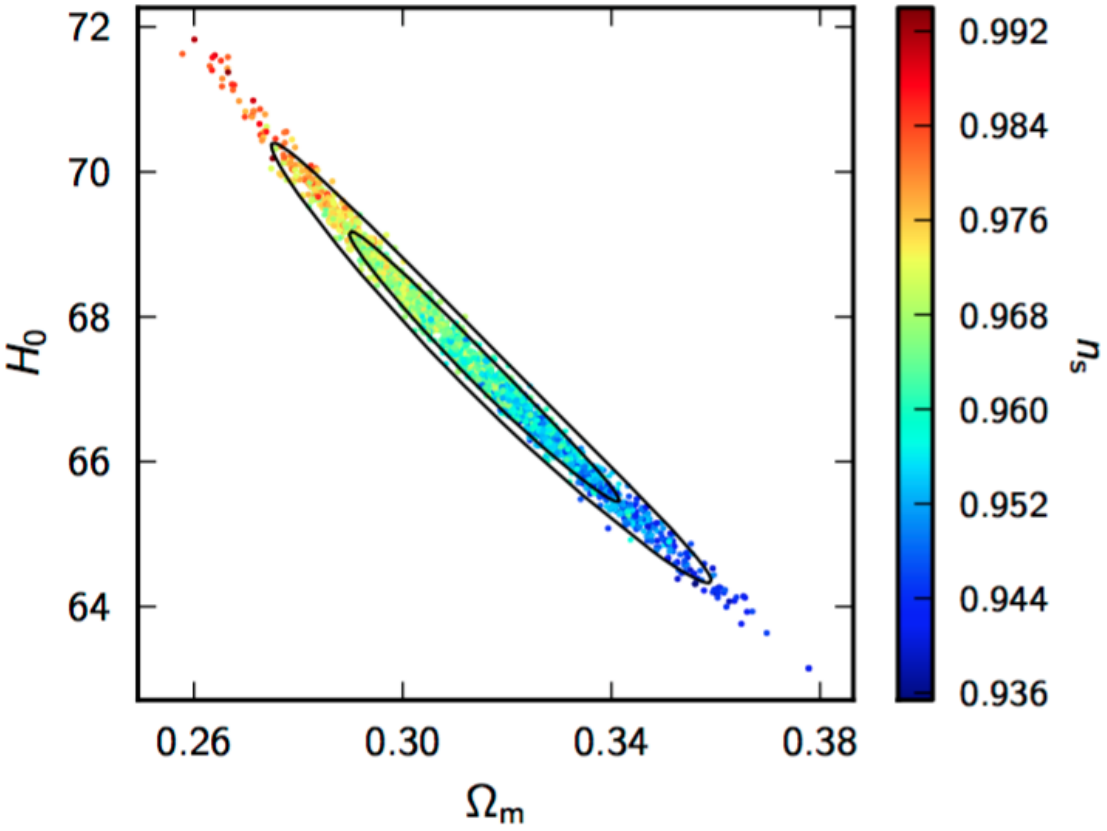

Figure 2.2. Degeneracy between Ω_M and H_0 as illustrated in [16].

are converted to the 3-dimensions in real distances using a fiducial cosmology, usually the one constrained by CMB anisotropy analysis. Then the statistical information on the *baryon acoustic oscillations* (BAO) is extracted in the form of the correlation function,

$$\xi(r) = \frac{1}{V} \int d^3x \delta(x) \delta(x + r) \tag{2.1}$$

where $\delta(x)$ is the density field. Correlation is a function of r only, the distance between two points on the density field, due to statistical homogeneity and statistical isotropy. The Fourier transform of correlation function gives the power spectrum of matter densities; an equivalent measure used in literature.

From the CMB anisotropy power spectrum one can estimate the angular diameter distance to the last scattering surface with use of the preferred angular sizes in the data.

The galaxy power spectrum also brings in such preferred scales, but unlike CMB, the galaxy counts are done in a survey volume. So the preferred length scales are not directly relatable to the angular size; they are also sensitive to the inhomogeneity distributions in the radial direction and therefore to $H(z)$. As a result, instead of measuring $\Delta\theta$ we can only measure the cube root of some volume element $(\Delta\theta^2\Delta z)^{1/3}$. Using geometrical arguments it is possible to come up with a distance measure, *volume distance*, a combination of angular dimeter distance $d_{\rm A}(z)$ and $H(z)$,

$$D_{\rm V} = [(1+z)^2 d_{\rm A}^2 cz/H(z)]^{1/3} \tag{2.2}$$

A recent *BAO Hubble diagram* can be seen in Figure 2.3 from [17].

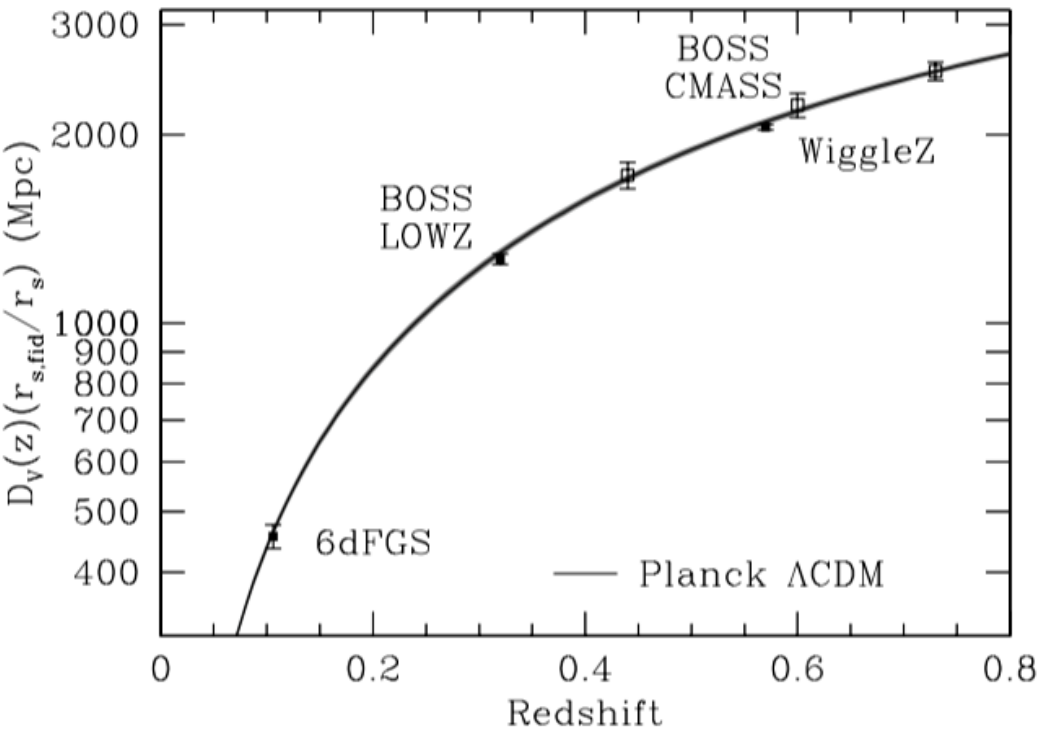

Figure 2.3. A recent BAO Hubble diagram. Each survey measures $D_{\rm V}$ around a pivoting redshift value, so it is possible to plot $D_{\rm V}$ vs z diagram. Adapted from [17].

Quasar spectra measured in galaxy redshift surveys became crucial for cosmology. During its long time of travel, quasar light undergoes Lyman-α absorption by Hydrogen atoms when it passes through a matter overdensity. During that time universe keeps

expanding, which redshifts the absorption line. So matter overdensities far away appear as absorption lines at higher wavelength in the quasar spectrum, and we get very precise information on the inhomogeneities along the line-of-sight. So the power spectrum is obtained in a one dimensional redshift space and characteristic scales are only related to $H(z)$. This is important in breaking the degeneracy between $d_{\rm A}(z)$ and $H(z)$ which is present in galaxy redshift surveys as mentioned before and the Lyman-α forest can measure the Hubble parameter at a very high redshift (Figure 2.4).

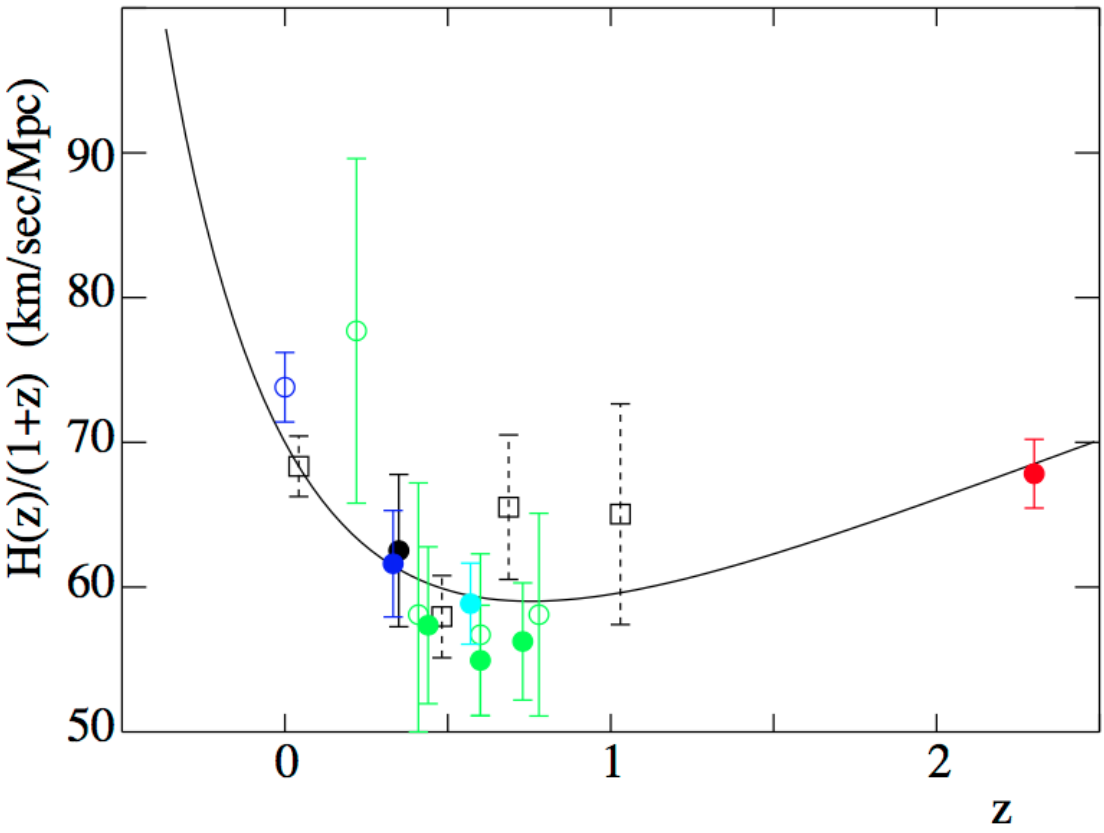

Figure 2.4. Hubble parameter estimation through galaxy power spectra (blue, green, black) requires additional information on $d_{\rm A}(z)$. Lyman-α data (red) however can give $H(z)$ by themselves. Results are consistent with an early deceleration. Adapted from [18].

3. EXPANSION OF SPACE: WHAT CAN WE GET FROM OBSERVATIONS?

3.1. Mathematical Framework and Motivation

Simply put, the observations found supernovae at a given redshift z to be *fainter* than what would be expected even for an empty flat universe, i.e. for one with $a(t) \propto t$, that is, with zero acceleration/deceleration. This faintness puts the sources farther away as compared to the empty universe, hence farther back in time, due to the constant speed of light. On the other hand, by Eq. 1.10 the redshift gives the size of the universe at the emission of the light, hence the faintness pushes the bottom of the a vs. t curve to the left, hence acceleration.

The original works [10, 11] used the ΛCDM model, i.e. assumed that the universe is dominated by matter [corresponding to a perfect fluid with equation of state (EoS) $p = 0$; and some of it possibly dark, although this does not matter for the Einstein equations], since we know that matter exists in the universe, and a cosmological constant (corresponding to a perfect fluid with EoS $p = -\rho$) as the agent causing the acceleration. They parametrised the contributions of matter and cosmological constant as Ω_{M} and Ω_{Λ}, and performed fits of the data to the $d_L(z)$ functions calculated for assumed values of these parameters. On the Ω_{M}-Ω_{Λ} plane (Figure 3.1), the best fits they found suggested that $\Omega_{\Lambda} - \Omega_{\mathrm{M}} \simeq 0.4$, consistent with an accelerating universe. The best fits give very weak constraints on the sum $\Omega_{\Lambda} + \Omega_{\mathrm{M}}$ determining the curvature of the universe, however; that quantity was first meaningfully constrained by the measurement of the location of the first peak in the power spectrum of the fluctuations in the cosmic background radiation [16].

However, the procedure of going from a predicted $a(t)$ to a predicted $d_L(z)$ can in principle be inverted, if we derive lookback time $(t_0 - t)$ in terms of $d_L(z)$. Equation

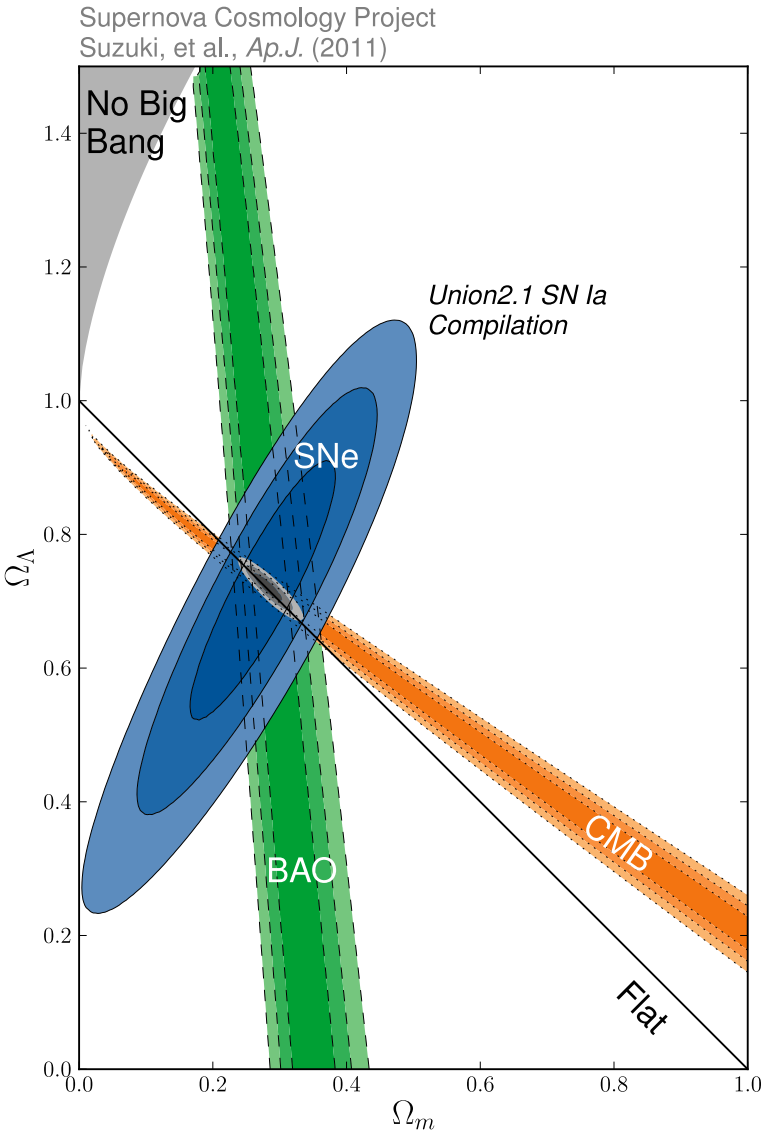

Figure 3.1. Parameter space for a ΛCDM universe with constraints from various observations.

1.17 can easily be rewritten as

$$f\left(\frac{d_L(z)}{a_0(1+z)}\right) = c\int_t^{t_0}\frac{dt'}{a(t')} \tag{3.1}$$

Taking derivatives of both sides with respect to z,

$$f'\left(\frac{d_L(z)}{a_0(1+z)}\right)\frac{1}{a_0}\frac{d}{dz}\left(\frac{d_L(z)}{1+z}\right) = -c\frac{dt}{dz}\frac{1}{a(t)} \tag{3.2}$$

Now we can replace f' from (1.6) and $a(t)$ from (1.10). After rearranging terms we see

that first integral gives,

$$t_0 - t = \int_0^z \frac{dz}{c(1+z)} \frac{1}{\sqrt{1 - \kappa \frac{d_L^2(z)}{(1+z)^2}}} \frac{d}{dz} \left[\frac{d_L(z)}{1+z} \right] \tag{3.3}$$

where the curvature κ is defined by

$$\kappa = \frac{k}{a_0^2} \tag{3.4}$$

hence is a parameter that can take continuous values.

As mentioned above, we keep the κ-term, since the SNe Ia data do not tell us that the universe is flat (or otherwise). Once $t(z)$ is determined, this function can in principle be inverted to give $z(t)$.

Hence, if we have good knowledge of the function $d_L(z)$ and if the integration (3.3) and subsequent inversion can be performed analytically, we would have a good candidate for an analytical expression for the expansion history of the universe via Eq. 1.10. Then the derivatives of that function would reveal the history of the Hubble parameter and periods of acceleration or deceleration.

Since no theory of gravity (Einstein or modified) or assumption about the content of the universe is used, this is called a *model-independent approach*, or since the emphasis is on simply determining the unknown metric function of the universe, occasionally cosmography [3].

In this chapter[2] we follow this approach. We fit families of functions to the $d_L(z)$ data, and determine the best fitting member of each family. The choice of function families is not motivated by a physical model we have in mind, rather, by possible simplicity of the analytical operations. Trying to find good fits to $d_L(z)$ rather than to $a(t)$, or some combination of its derivatives such as the deceleration parameter

[2]The material of this chapter was published as [19].

$q = -a\ddot{a}/\dot{a}^2$, etc. is better-motivated, since the observationally measured function is $d_L(z)$. We also use alternative redshift variables in addition to the conventional redshift z, introducing one of our own, and denoting them by y_i. We compare goodness of fit of the results with each other, and in particular, with the standard model of cosmology, the ΛCDM model. We find that none of the models we investigated fits meaningfully better than ΛCDM.

Then we attempt to extract all the possible information about the expansion history of the universe, including periods of acceleration and deceleration. It turns out that not much analytical progress can be achieved in terms of the time t, but both the first and second time-derivatives of the scale function $a(t)$ can be evaluated *in terms of a redshift variable* y_i analytically, once an analytical result for $d_L(y_i)$ is assumed. We find that while the SNe Ia data *strongly suggest* that the present acceleration of the universe is positive, they *by themselves* cannot tell us that the universe was decelerating in the past. However, we find that including the GRB luminosity-distance data improves the situation, even though they are much fewer in number, subject to much larger uncertainties, and not *really* model-independent. We also rederive the result that *for given* $d_L(y_i)$, the present value of acceleration of the universe is independent of its curvature.

When we finally *do* use Einstein's Equations to derive conclusions about the content of the universe in the past according to General Relativity, we find that there is a special value of redshift at which the density of the universe is independent of its curvature *for a given* $d_L(y_i)$. We use this fact to put an upper limit on the matter density of the universe, leading to a lower limit on dark energy. We also investigate the evolution of the total EoS parameter, all analyses performed *using only the SN+GRB data without using an EoS for the cosmic fluid.*

3.2. Fitting the luminosity distance function

3.2.1. Alternative variables

The conventional redshift z is not the only possible redshift variable, not necessarily even the best variable to work with. Cosmography has usually been the effort to extract as many Taylor expansion coefficients as possible of various cosmological functions as functions of time or redshift; for example, the Hubble and deceleration parameters as first and second terms. But one look at Eq. 1.10 shows that the radius of convergence of the Taylor series for $a(z)$ is 1, hence some such Taylor series will not be reliable beyond $z = 1$ [3]; and alternative redshift variables have been used in the literature [3, 20]. We will use these variables too, and introduce one of our own.

We will occasionally denote the conventional redshift z by y_0. The first alternative variable is [3]

$$y_1 = \frac{z}{z+1} \tag{3.5}$$

other alternatives introduced in [20] are

$$y_2 = \arctan\frac{z}{z+1} \qquad y_3 = \frac{z}{z^2+1} \qquad y_4 = \arctan z \tag{3.6}$$

we introduce[3]

$$y_5 = \ln(z+1) \tag{3.7}$$

and also will use the almost-trivial $y_6 = u = z + 1$.

Behaviours of the different redshift variables as function of the scale factor are shown in Figure 3.2. It can be seen that y_3 does not change monotonically with z,

[3]During the writing of this manuscript, we became aware of another work [21] introducing the same variable.

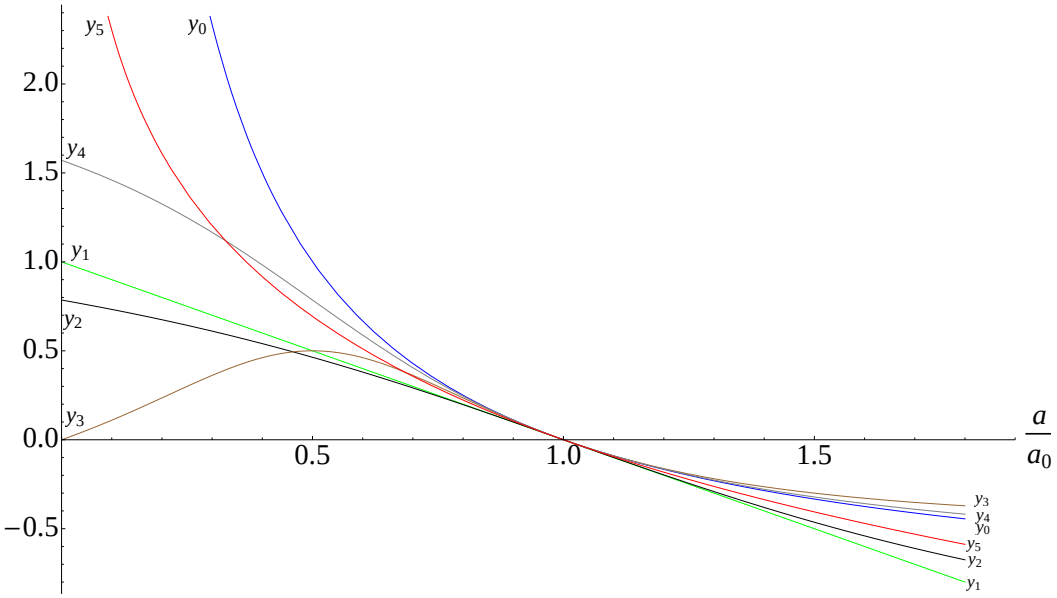

Figure 3.2. Relation betweeen the redshift variables y_0-y_5 and the scale factor. Note that y_3 is not monotonic with a.

therefore $a(t)$, hence we will not use that variable.

3.2.2. The candidate families and the fits

Analytical forms of $d_L(z)$ for simple models can be calculated from (1.17); for example, for the flat matter dominated model one gets

$$d_L(z) = c\frac{2\sqrt{z+1}}{H_0}(\sqrt{z+1}-1) \tag{3.8}$$

whereas for the flat Λ-dominated model, one gets

$$d_L(z) = c\frac{z(z+1)}{H_0} \tag{3.9}$$

There is no analytical solution for cosmologies with more than one fluid. However it can be evaluated for a single fluid with a constant equation of state even in a curved space;

$$d_L(z) = \frac{c(1+z)}{2H_0\sqrt{\Omega_K}}\left(B(z)^{2/(1+3w)} - B(z)^{-2/(1+3w)}\right) \tag{3.10}$$

where

$$B(z) = \frac{(\sqrt{\Omega_K} - 1)(1+z)^{(1+3w)/2}}{\sqrt{\Omega_K} + \sqrt{\Omega_K + (1-\Omega_K)(1+z)^{(1+3w)}}} \tag{3.11}$$

To determine candidate functions for $d_L(y_i)$, we choose 8 families of functions (See Table 3.1) to fit to the data, that is, the Union 2.1 dataset [12], with fitness assigned by χ^2 minimisation. But we want a model-independent analysis and therefore need to make choices as generic as possible; hence we start with polynomials with no constant term [except when using $y_6 = u = z+1$, when the constant term is determined in terms of the coefficients of the other powers such that $d_L(u = 1) = 0$]. The second and third families are polynomials multiplied by an exponential function where the exponent is linear and quadratic in y_i, respectively. We extend the spectrum by introducing three more families which are the first three families multiplied by $1 + z$; this is done to simplify (3.3) where division of d_L by $1 + z$ is present. Of course, when an alternative redshift variable is used, this factor is expressed in terms of that variable, e.g. $(1-y_1)^{-1}$. One further generalisation of polynomials is the Padé approximant [22–24] which is given by

$$\text{Pade}(y, M, N) = \frac{P_M(y_i)}{1 + P_N(y_i)} \tag{3.12}$$

where $P_M(y_i)$ is the M^{th} order polynomial with constant term set to zero; and we have added one family consisting of Padé approximants multiplied by $(1 + z)$.

For each family, we determine the best-fitting member, i.e. the one with the lowest $\chi^2_\nu \equiv \chi^2/\text{d.o.f}$ value. As an illustration, in Figure 3.3 we show the Union 2.1 data (in terms of luminosity distance and standard redshift $z \equiv y_0$); the N=2 to 7 fits for the first family, i.e. simple polynomials; the curves for the flat matter-dominated model of the 1990's (based on the H_0 value derived from the data) and the best-fitting ΛCDM model; and the one-sigma confidence-levels of the best-fitting member of the family F1. We can see that the matter-dominated model is comfortably excluded,

Table 3.1. The 8 different families used in fits. y can be any one of the redshift parameters described in Sect. 3.2.1, $P_N(y)$ is the N^{th} order polynomial with zero constant term (except when using $y_6 = u$, see Sect. 3.2.2), $u(y)$ is $(1 + z)$ expressed in terms of y, Pade(y, M, N) is the Padé approximant in variable y and orders M & N; and c & d are constants.

Designation	Function family
F1	$P_N(y)$
F2	$P_N(y)u(y)$
F3	$P_N(y)\exp(cy)$
F4	$P_N(y)u(y)\exp(cy)$
F5	$P_N(y)\exp(cy + dy^2)$
F6	$P_N(y)u(y)\exp(cy + dy^2)$
F7	Pade(y, M, N)
F8	$u(y)$ Pade(y, M, N)

and the strange behaviour of F17 illustrates the potential of overfitting. The best-fitting polynomial is the 4^{th} order one, telling us that no more than four independent cosmological parameters can be meaningfully extracted from the Union 2.1 data, if one expands the function $d_L(z)$ into a MacLaurin series.

Figure 3.4 shows the best-fitting members from each family, for the variable $z \equiv y_0$. The one-sigma confidence-levels are not shown in order not to clutter up the figure; they are similar to those in Figure 3.3, unless stated otherwise. Figures 3.5-3.9 are similar to Figure 3.4, but for the other redshift variables.

The full sets of best fits for each family and redshift variable are indicated in Table 3.2 and illustrated in Figure 3.10.

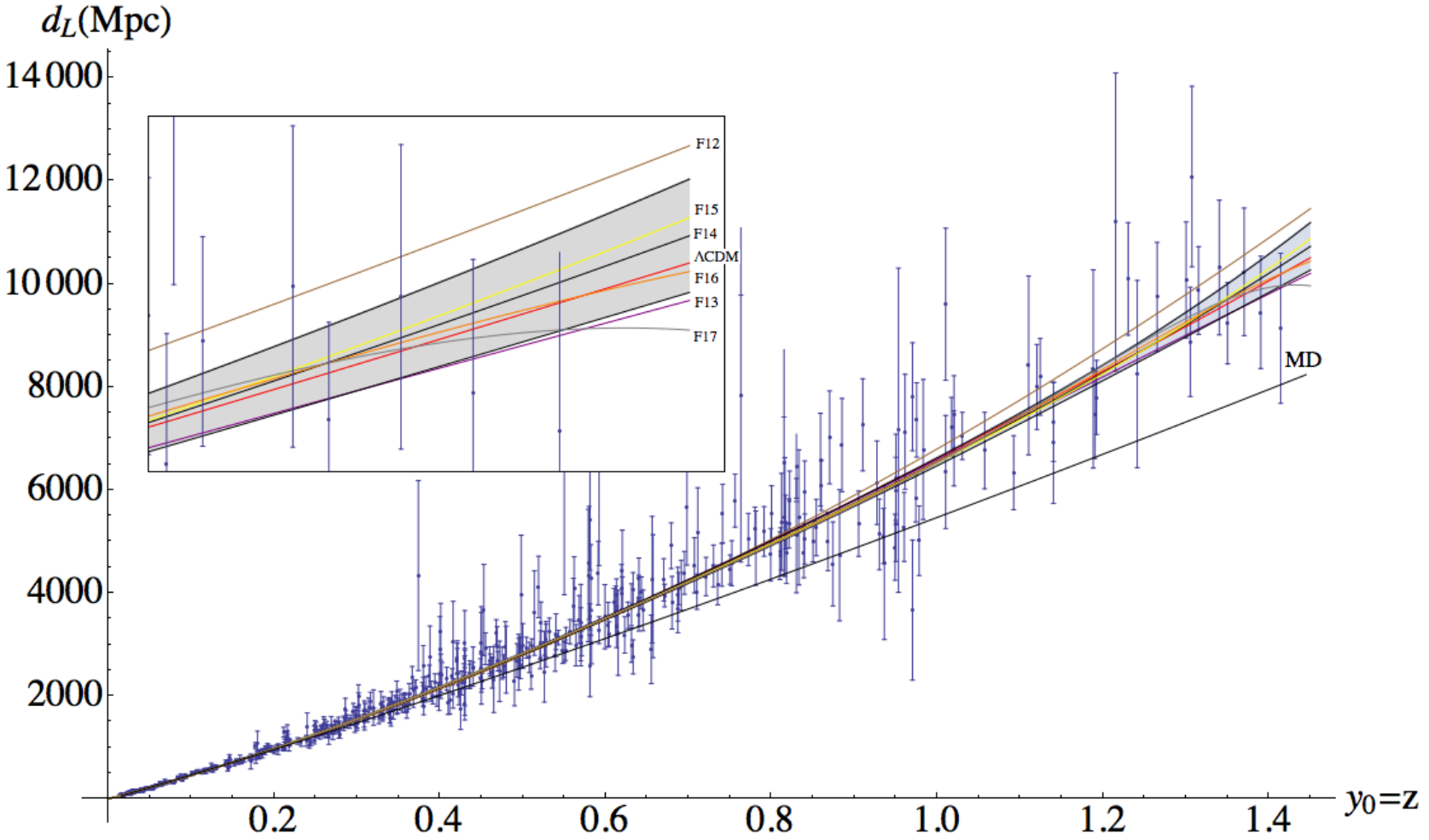

Figure 3.3. Union 2.1 data (in terms of luminosity distance and standard redshift $z \equiv y_0$); the N=2 to 7 fits for the first family, i.e. simple polynomials; the fits for the MD (black) and ΛCDM (red) models, and the one-sigma confidence-levels of the best-fitting member (N=4) of the family F1. The inset shows the right end, magnified. Note the strange behaviour of F17.

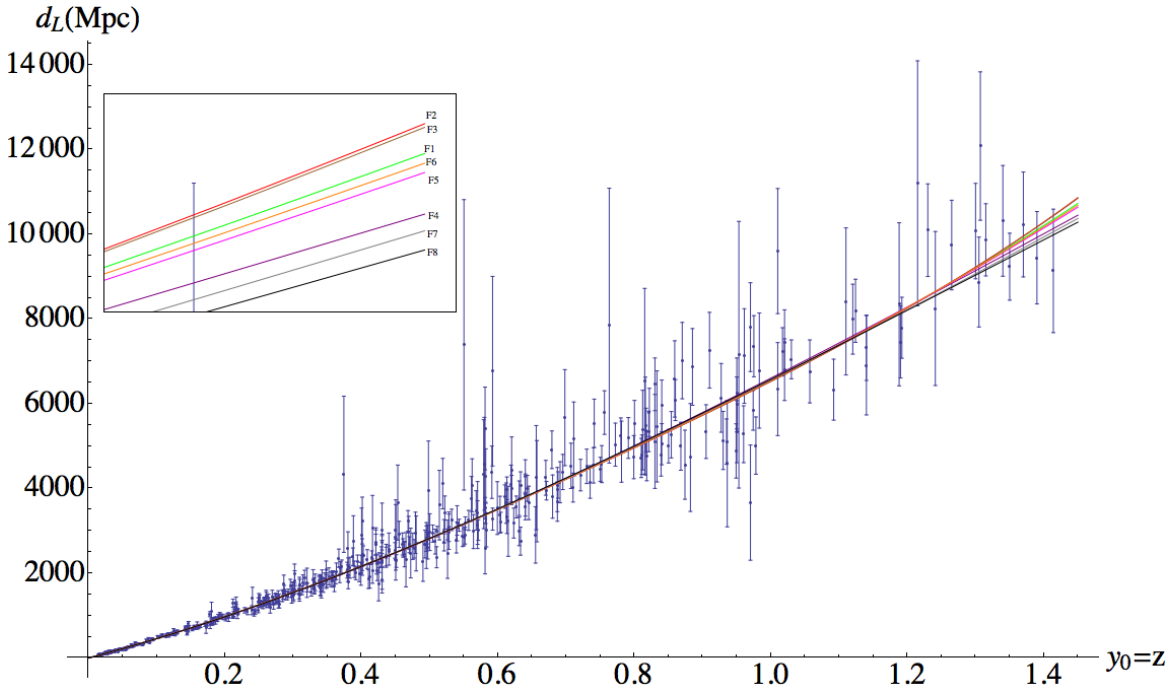

Figure 3.4. Union 2.1 data (in terms of luminosity distance and redshift $z \equiv y_0$); and best fits for each function family listed in Table 3.2. The one-sigma confidence-levels are not shown to not clutter up the figure; they are similar to those in Figure 3.3.

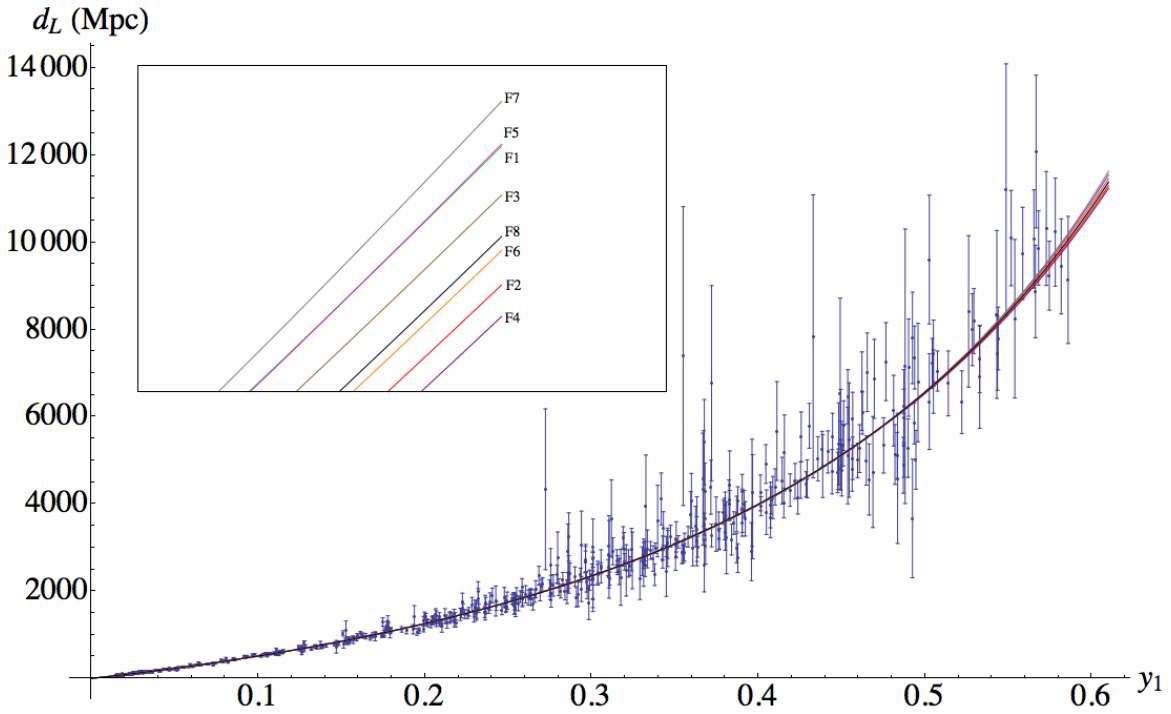

Figure 3.5. Same as in Figure 3.4 but with the redshift variable y_1.

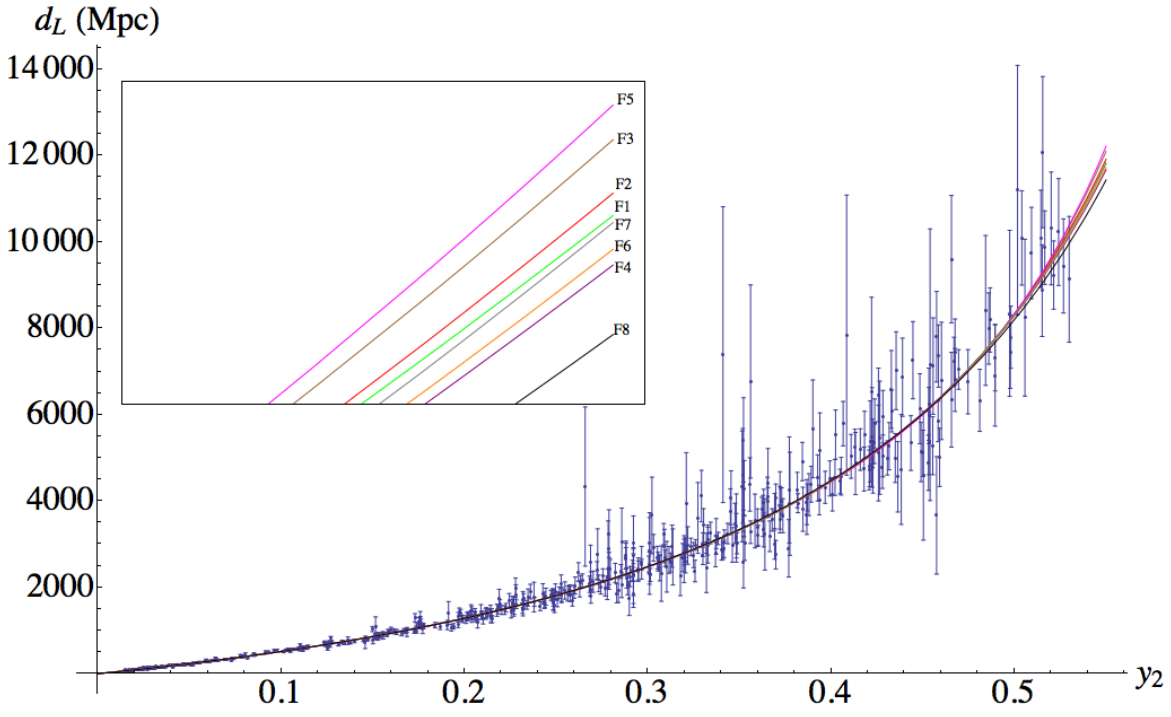

Figure 3.6. Same as in Figure 3.4 but with the redshift variable y_2.

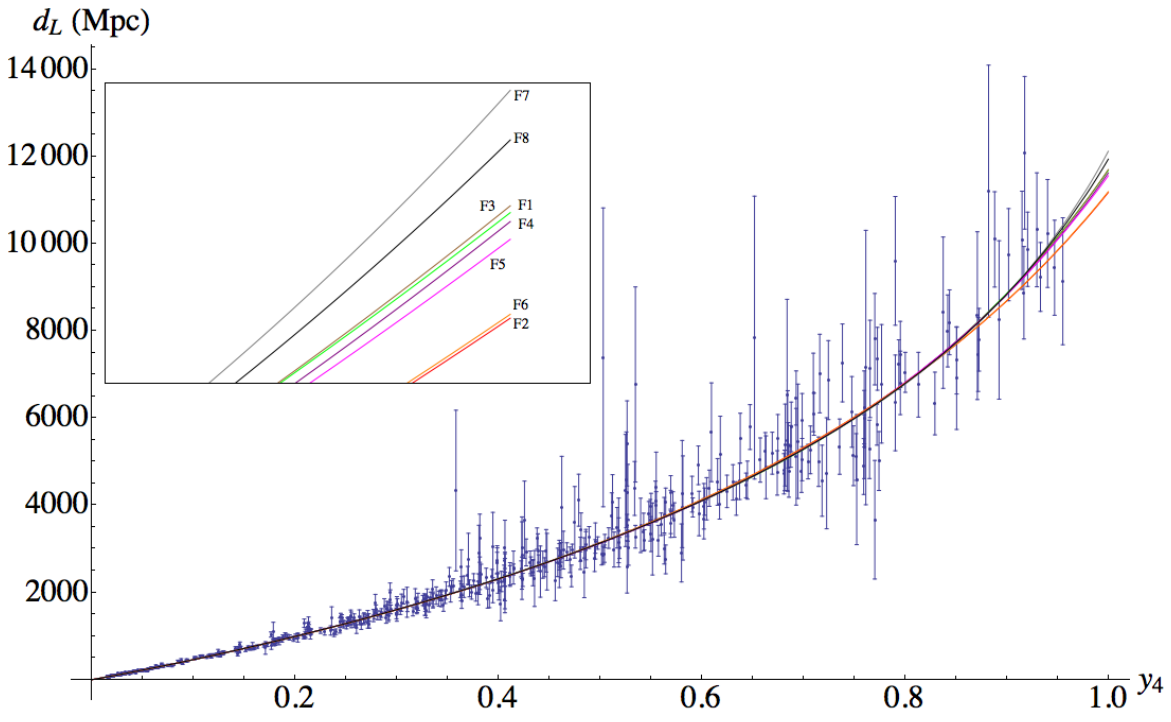

Figure 3.7. Same as in Figure 3.4 but with the redshift variable y_4.

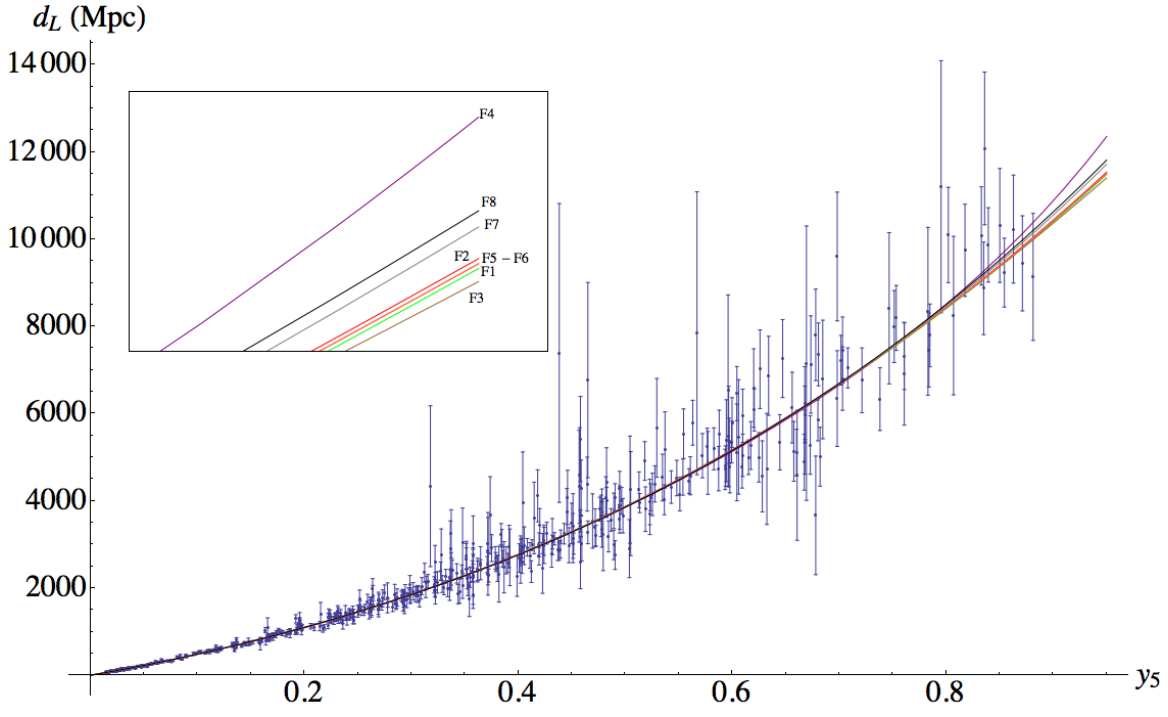

Figure 3.8. Same as in Figure 3.4 but with the redshift variable y_5.

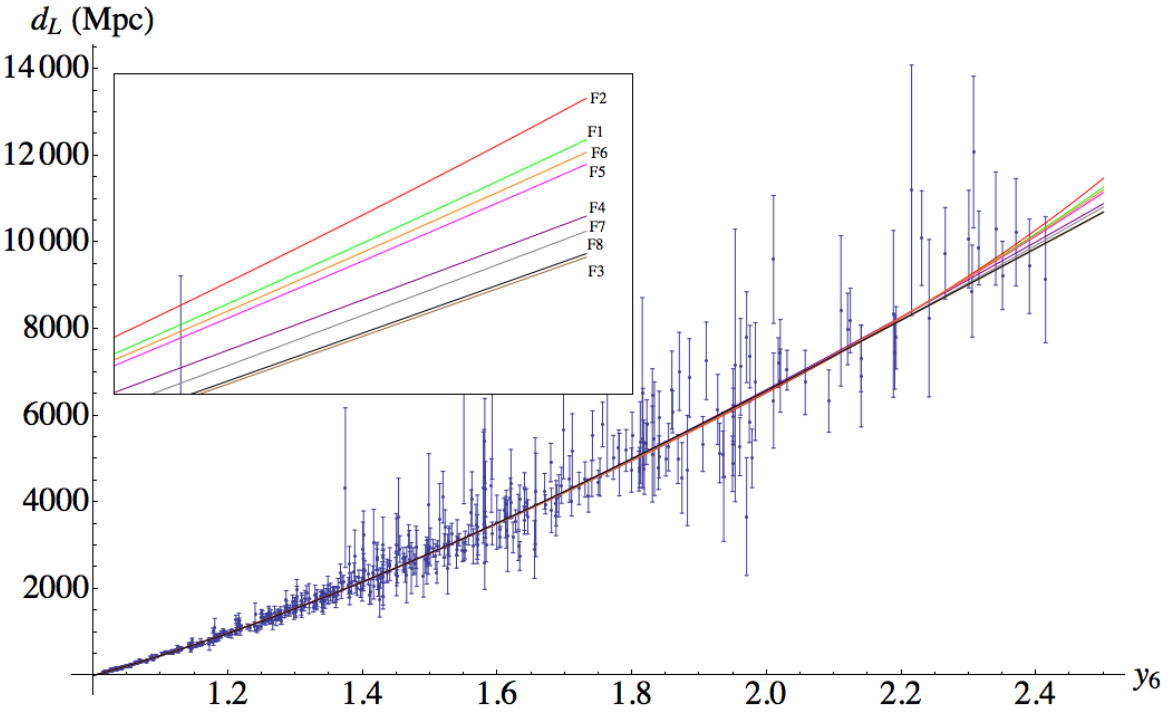

Figure 3.9. Same as in Figure 3.4 but with the redshift variable $y_6 = u = 1 + z$.

Table 3.2. The best fits for the Union 2.1 SNe Ia data. Each cell displays the internal label(s) of the best-fitting member of the row's family for the column's redshift variable, and the fit's $\chi^2_\nu \equiv \chi^2/\text{d.o.f}$ value. Note that $\chi^2_\nu = 0.9340$ for ΛCDM (the variable is $y_0 = z$).

family \ variable	$y_0 = z$	y_1	y_2	y_4	y_5	$y_6 = u$
F1	4; 0.9355	5; 0.9371	6; 0.9384	5; 0.9366	3; 0.9354	4; 0.9355
F2	4; 0.9353	3; 0.9353	5; 0.9367	3; 0.9360	3; 0.9353	4; 0.9353
F3	5; 0.9370	4; 0.9367	6; 0.9381	4; 0.9353	3; 0.9365	3; 0.9361
F4	2; 0.9357	2; 0.9340	4; 0.9365	4; 0.9358	4; 0.9354	2; 0.9357
F5	4; 0.9357	5; 0.9372	6; 0.9381	5; 0.9368	3; 0.9355	4; 0.9357
F6	4; 0.9356	3; 0.9351	3; 0.9358	3; 0.9359	3; 0.9355	4; 0.9356
F7	2;1; 0.9350	2;1; 0.9344	2;1; 0.9343	3;2; 0.9384	2;1; 0.9346	2;1; 0.9350
F8	1;2; 0.9364	2;1; 0.9350	1;1; 0.9339	2;2; 0.9370	2;1; 0.9348	1;2; 0.9364

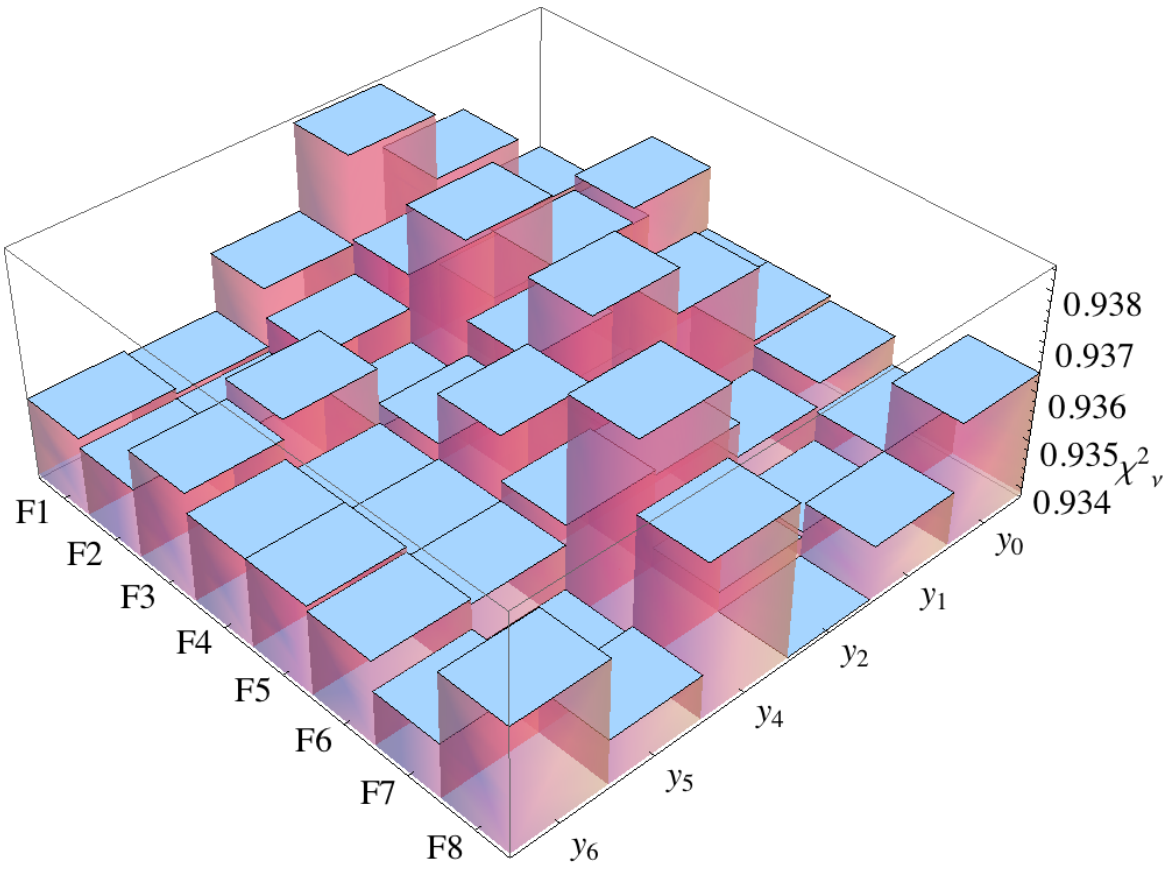

Figure 3.10. χ^2_ν values in Table 3.2, illustrated as a 3D bar chart for different function families and redshift variables.

We see from Table 3.2 that none of the fits is significantly better than the ΛCDM model. In fact, only one (F8, y_2) has a lower and one (F4, y_1) an equal χ^2_ν value; they range between 0.9339 and 0.9384, compared to ΛCDM's 0.9340 (with $y_0 = z$ as the independent variable). But, being the best fits in their respective families, they are not significantly worse either, so we will use all of them for the time being.

3.3. Determination of the expansion history of the universe

3.3.1. More on the procedure

As declared in the introduction to this chapter, what we would ideally like to do is to find $t(z)$ by performing the integration (3.3) for a given $d_L(z)$ function, then find $z(t)$ by inverting that result, hence find $a(t)$ by Eq. 1.10 [Of course, the same procedure can also be applied in terms of alternative variables y_i]. Unfortunately, for all but the simplest functions, neither the intergration, nor the subsequent inversion can be analytically performed. Numerical integration and inversion can provide numerical $a(t)$ functions, but numerical differentiation of these is problematic, hence not very useful.

However, for a given $d_L(z)$, the time-derivatives of $a(t)$ can be calculated *analytically* in terms of the redshift variable(s):

$$\dot{a} = \frac{da}{dt} = \frac{da}{dz}\frac{dz}{dt} \tag{3.13}$$

i.e. as the z-derivative of (1.10) divided by the integrand in (3.3). Similarly,

$$\ddot{a} = \frac{d}{dt}\dot{a} = \frac{d\dot{a}}{dz}\frac{dz}{dt} \tag{3.14}$$

Furthermore, one can plot (but not write) $\dot{a}$ and $\ddot{a}$ as functions of time, since $z(t)$ can be evaluated numerically by integration, which is a robust procedure.

We also noted in the Introduction that the SNe Ia data are meaningful for any value of curvature; hence the expression dz/dt, coming from Eq. 3.3 and used in eqs.(3.13) and (3.14) contains the curvature κ. We choose $\kappa_0 = (10000\ \mathrm{Mpc})^{-2} \sim (2\mathrm{c}/\mathrm{H}_0)^{-2}$ as the upper limit to positive curvature; 10000 Mpc is also approximately the maximum $d_L(z)$ value in the Union 2.1 data. We perform the procedure for κ values between $-\kappa_0$ and $+\kappa_0$, in $0.2\kappa_0$ increments, i.e. we take $\kappa = k'\kappa_0$, with $-1 \leq k' \leq +1$.

Incidentally, the current value of the Hubble parameter can be extracted from $d_L(z)$ as

$$H_0 = \left.\frac{\dot{a}}{a}\right|_{z=0} = \frac{c}{\left.\frac{d}{dz}\left[\frac{d_L(z)}{1+z}\right]\right|_{z=0}} \tag{3.15}$$

and similar expressions can be written in terms of the other redshift variables. We find $H_0 = 70.55 \pm 0.62 \frac{\mathrm{km/s}}{\mathrm{Mpc}}$, using all best fits in Table 3.2.

3.3.2. Determination of time derivatives of the scale function

The use of 6 different redshift variables and 8 function families for approximating $d_L(z)$ gives 48 possible representations of the expansion history of the universe. When we plot the possibilities for the scale function $a(t)$ in a 6×8 grid (Figure 3.11), the repesentations are visually virtually identical, and not very informative. The $\dot{a}(z)$ plots shown in Figure 3.12 are a bit more meaningful visually, but the really visually informative plots are those of acceleration, $\ddot{a}$, where sign changes are more apparent (Figure 3.13). All these plots were made for 11 different spatial curvature values chosen as described previously.

But, problems with the $\ddot{a}(z)$ plots strike the eye at first look. Many of the plots show unnatural-looking fluctuations; especially divergences at high y_i due to differentiating the d_L twice: Powers of z with coefficients arranged to mostly cancel each other do not do so when those coefficients are changed due to differentiation. As a result, some models would seem to suggest negative acceleration today, while some

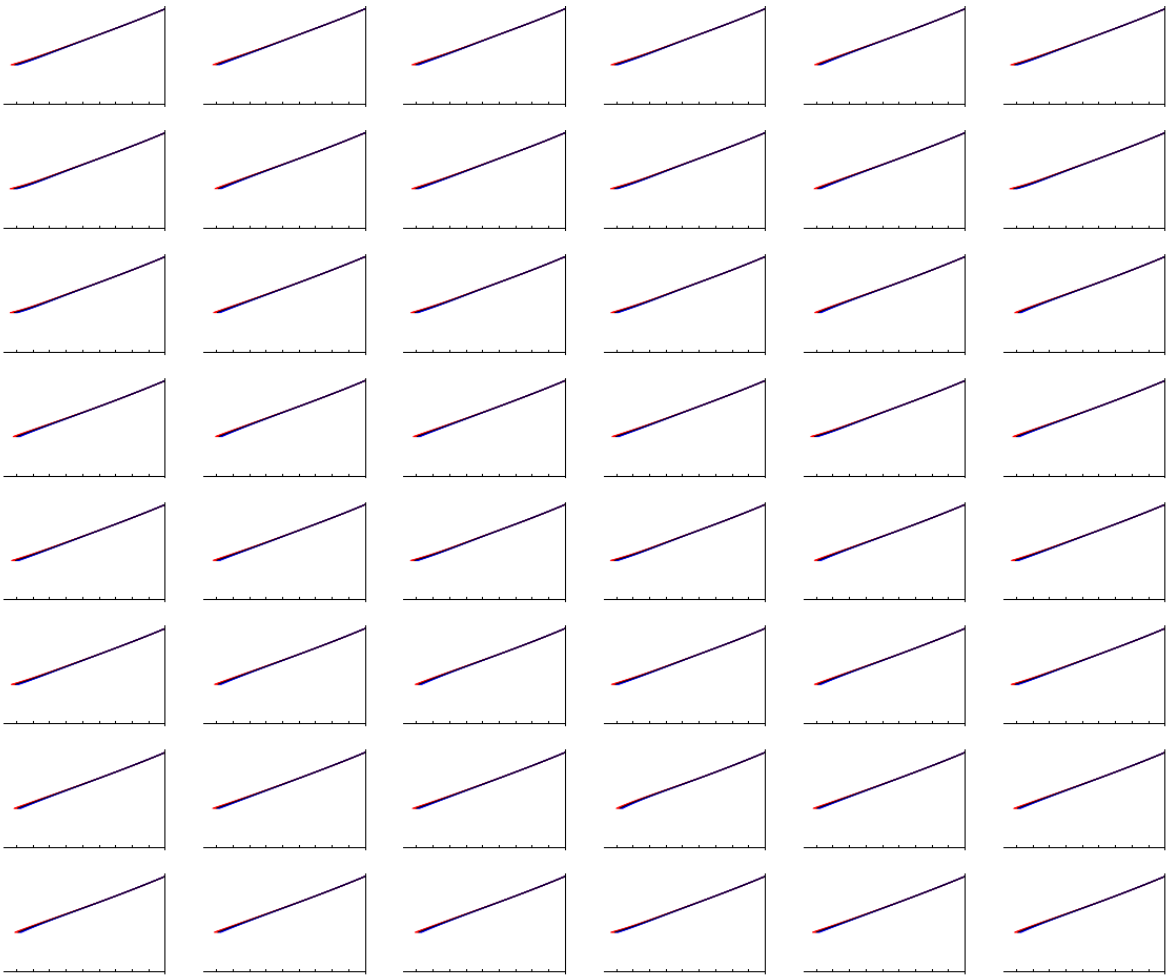

Figure 3.11. The $a(t)$ functions, computed by numerical integration of Eq. 3.3 and subsequent numerical inversion to find $z(t)$ (or similar analysis with one of the redshift variables y_i), using the fits found for $d_L(y_i)$ to the Union 2.1 data. The columns represents analyses with y_0, y_1, y_2, y_4, y_5 and u, respectively, and rows are for candidate families F1-F8. In each plot, the horizontal axis is t, ticked at 1 Gyr intervals, and the vertical axis is $a(t)$, normalized to 1 at the present epoch shown at the right end of each plot. For curvature, the same color-coding is used as in Figure 3.12, but the curves for different curvatures practically overlap in this figure.

others show positive acceleration in the past. So one can see that using the current SNe Ia data in a model-independent way, one cannot tell the value, or even the existence of the transition redshift; as also discussed in [21, Appendix A], and references therein, conclusions can heavily depend on the choice of parametrization (see however, [25] for a dissenting view).

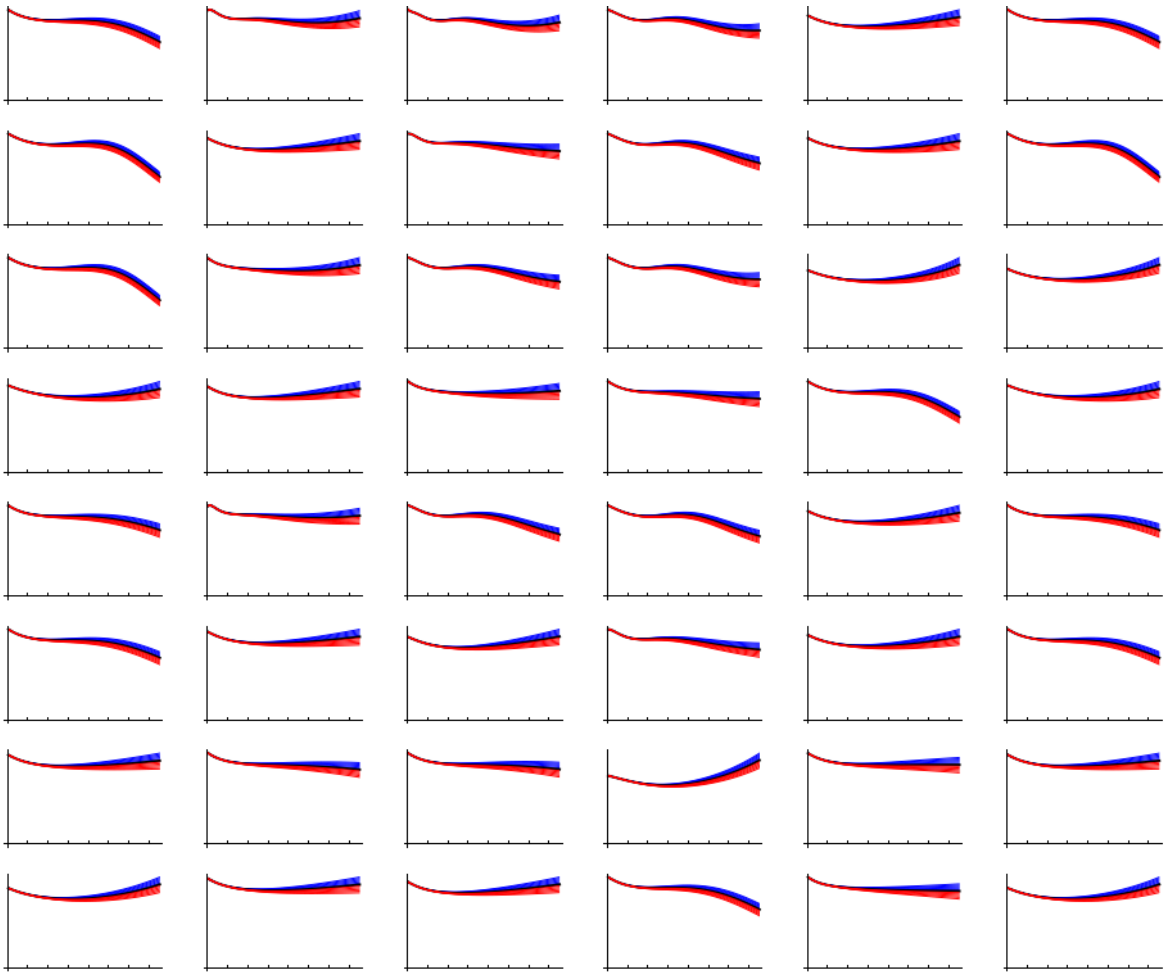

Figure 3.12. The $\dot{a}(z)$ functions, computed analytically for the Union 2.1 data by Eq. 3.13 or its analogs for the different redshift variables y_i. The columns and rows have the same meaning as in the previous figure. Blue, red and black curves represent open, closed and flat spaces respectively, with the range $-\kappa_0 \leq \kappa \leq \kappa_0$. For comparison purposes, the horizontal axes are transformed to be $z = y_0$, ticked with intervals $\Delta z = 0.2$, and $\dot{a}(0)$ is normalized to 1 in $(H_0 a_0)$ units.

In terms of showing least amount of unnatural fluctuations, the best variable seems to be the newly suggested redshift variable y_5, (the fifth column) the variables y_2 and y_4 showing significantly more fluctuations. One might speculate if this has to do with these variables being related to a/a_0 via trigonometric relations. Among the functional forms for $d_L(y_i)$, least amount of unnatural fluctuations in $\ddot{a}(z)$ are featured by the families featuring the Padé approximant (the two lowest rows).

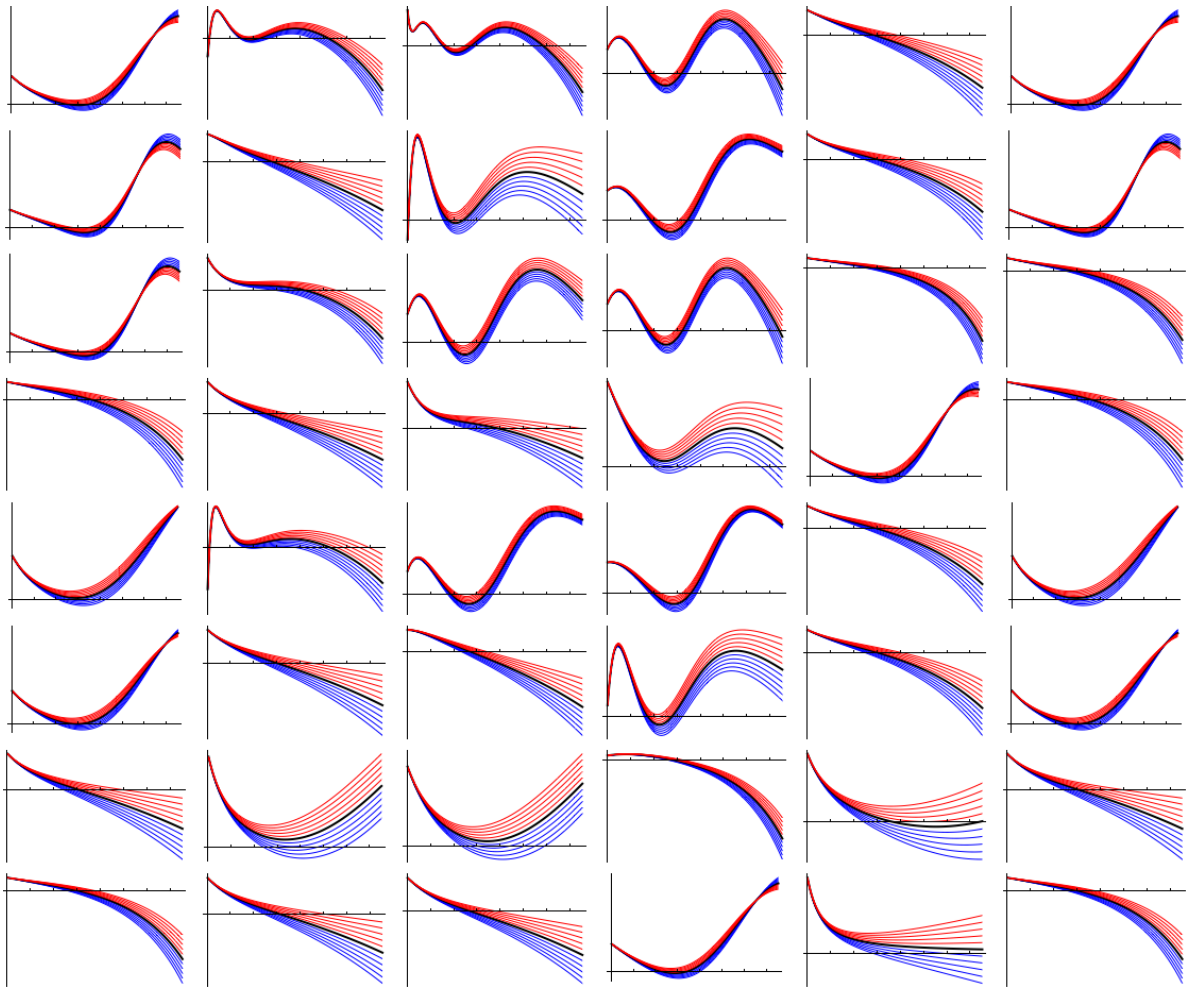

Figure 3.13. All $\ddot{a}(z)$ functions, computed analytically to the Union 2.1 data by Eq. 3.14 or its analogs for the different redshift variables y_i. The columns, rows and colors have the same meaning as in the previous figure. For comparison purposes, the horizontal axes are transformed to be $z = y_0$, ticked with intervals $\Delta z = 0.2$, and the vertical axes are in arbitrary units.

This last statement gives a hint to the source of the problem: All but the last two families in Table 3.1 have a polynomial as a factor, and polynomial fits to a set of data quickly diverge away from the visual data pattern just outside the interval with the data; due to the dominance of the highest powers at large magnitudes of the independent variable. Absence of this behavior is the main advantage of the Padé approximation over truncated MacLaurin series (e.g. [26]).

This divergence can be tamed by using data in a wider interval, if available. In our case, data extending to $z \sim 6$ *are* available as gamma ray burst [13] and quasar [14]

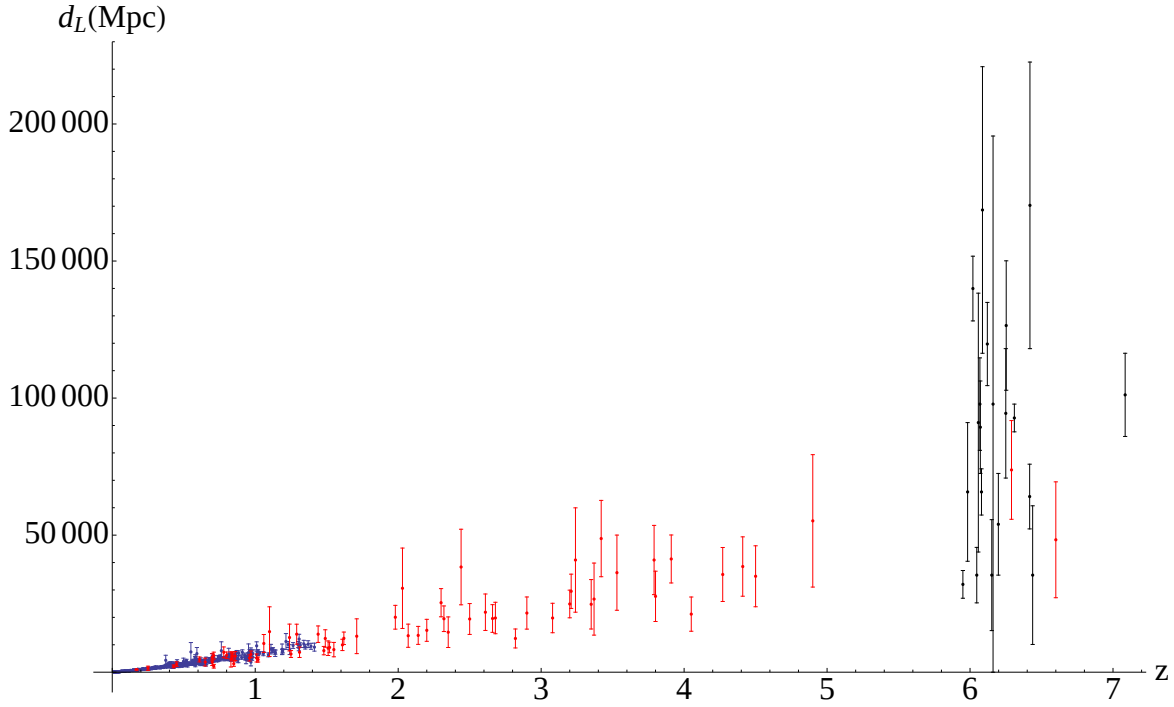

Figure 3.14. The Union 2.1 supernova data, shown in blue, the GRB data [13], shown in red, and the quasar [14] data shown in black, together.

data (Figure 3.14), but these actually are not suitable for model-independent analysis: They are called *standardisable* candles, and are not really standard candles, as discussed in the previous chapter. They also have large errors. Nevertheless, they can serve the purpose of taming the divergence of polynomials, while their large errors will give them little weight in the fits, hence they will not contaminate the analysis *very much* with physical model assumptions.

Unfortunately, the variations in the quasar data are too big: Incorporating them in our data set increases the χ^2_ν value to unacceptably large values, around 1.2. They are also concentrated near $z \sim 6$, whereas the GRB data are spread over the whole range $0 < z < 7$. Therefore we choose to incorporate only the GRB data consisting of 69 GRB's. Their addition to the 580 SNe Ia data modifies the plots of $\ddot{a}$ to give Figure 3.15; and the χ^2_ν values in Table 3.3 and Figure 3.16. It can be seen that the unnatural fluctuations have disappeared from most of the plots. Moreover, deceleration in the remote past can be seen in all the plots, unlike in Figure 3.13. As in that figure, the fifth column and seventh row are free from unnatural fluctuations, but so are the the

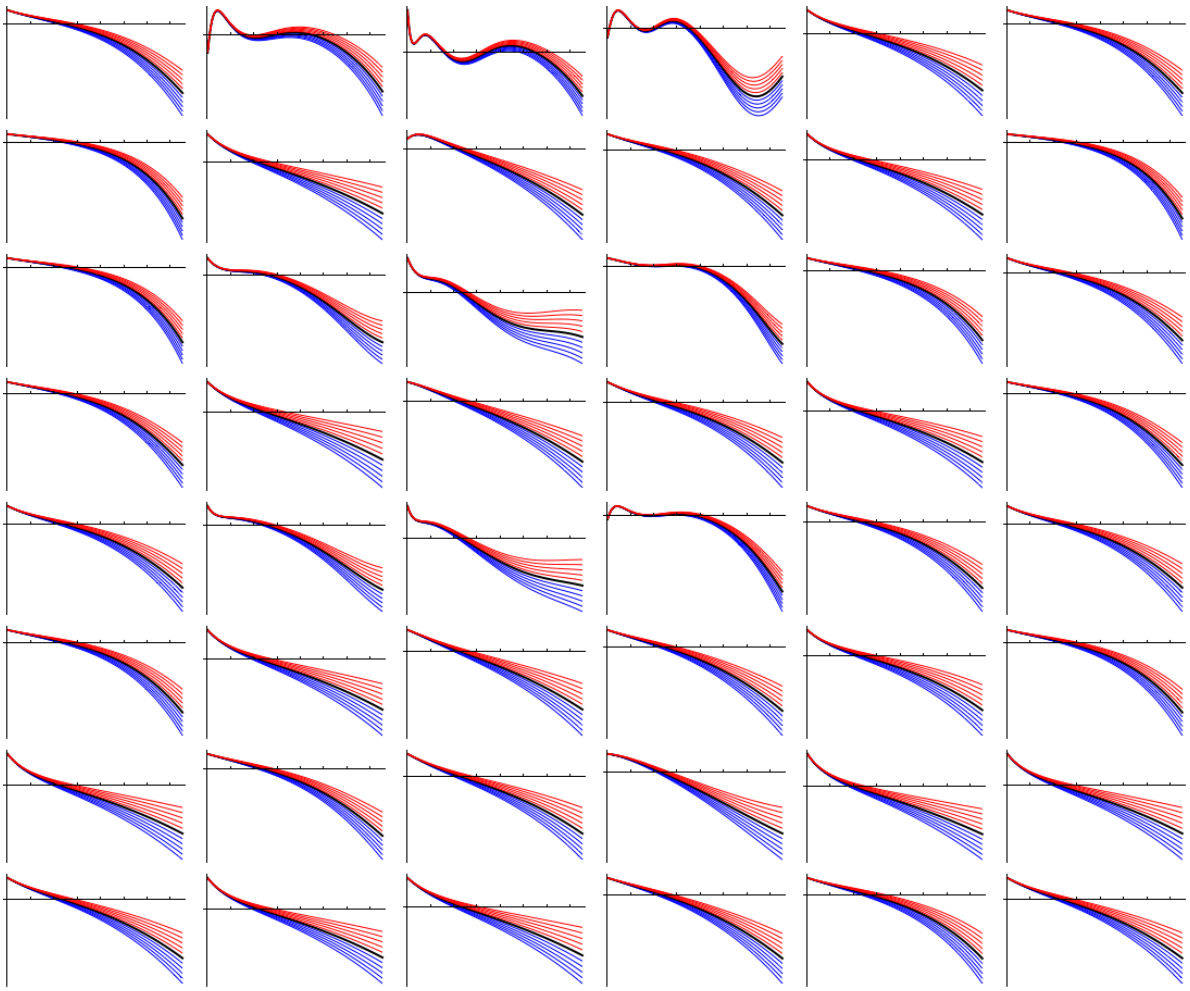

Figure 3.15. The $\ddot{a}(z)$ functions, computed analytically by Eq. 3.14 or its analogs for the different redshift variables y_i. The rows, columns and color coding have the same meaning as in Figures 3.11-3.13, fitted to the Union 2.1 and GRB data. For comparison purposes, the horizontal axes are transformed to be $z = y_0$, ticked with intervals $\Delta z = 0.2$,and the vertical axes are in arbitrary units.

first and sixth columns; and the second, fourth, sixth and eighth rows. Interestingly, presence of the factor $u(y) = 1+z$ improves the fit. In fact, in almost every cell of rows two, four and six of Table 3.2, the χ^2_ν value is smaller than the cell just above it. This motivated the addition of $u = z + 1$ as an extra redshift variable to the analysis (and of family F8). It turned out that this trivial-looking shift in the independent variable can serve as an illustrative example of the parametrization-dependence of conclusions refered to above, in the discussion of Figure 3.13: The best-fits for the third family are quite different! A close inspection of Table 3.2 reveals that after the variable shift, the

Table 3.3. The best fits for the Union 2.1 SNe Ia + GRB data. Each cell displays the internal label of the best-fitting member of the family for that row and the $\chi^2_\nu \equiv \chi^2/\text{d.o.f}$ value associated with the redshift variable for that column

variable / family	$y_0 = z$	y_1	y_2	y_4	y_5	$y_6 = u$
F1	5; 0.9540	5; 0.9591	6; 0.9616	7; 0.9594	3; 0.9529	5; 0.9540
F2	5; 0.9540	3; 0.9530	3; 0.9531	3; 0.9527	4; 0.9542	5; 0.9540
F3	6; 0.9550	6; 0.9569	6; 0.9588	6; 0.9560	4; 0.9536	5; 0.9543
F4	5; 0.9543	2; 0.9526	4; 0.9539	4; 0.9539	3; 0.9532	5; 0.9543
F5	4; 0.9530	6; 0.9567	6; 0.9583	7; 0.9564	5; 0.9543	4; 0.9530
F6	4; 0.9533	3; 0.9532	3; 0.9524	3; 0.9526	4; 0.9545	4; 0.9533
F7	2;1; 0.9534	2;3; 0.9545	1;2; 0.9526	3;2; 0.9551	2;1; 0.9539	2;1; 0.9534
F8	2;2; 0.9554	2;1; 0.9534	1;1; 0.9525	1;2; 0.9540	1;2; 0.9554	2;2; 0.9554

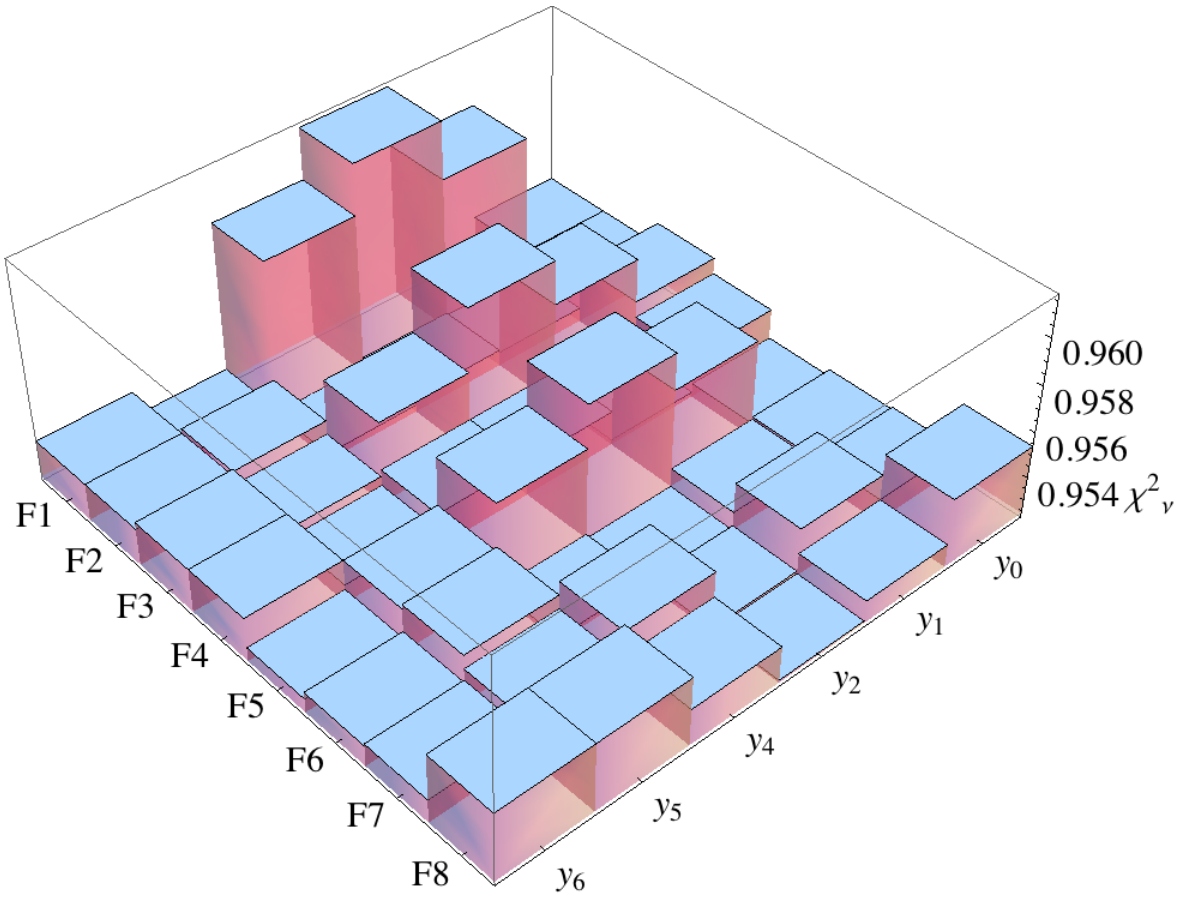

Figure 3.16. χ^2_ν values in Table 3.3, illustrated as a 3D bar chart for different function families and redshift variables.

three-parameter member of the family is the best fit, whereas it was the five-parameter one before. The results for the other families are not much affected, and the inclusion of the GRB data makes the difference much less drastic.

So, from here on in this work, we will use only the "more natural" fits, i.e. the fifteen fits belonging to columns one, five and six, and rows two, four, six, seven and eight of Figure 3.15. We show the average of these fifteen graphs in Figure 3.17. For the confidence interval, we take at each point the maximum of the confidence intervals of the fifteen curves. We do not apply the usual combination of errors technique, since these curves do not correspond to different "measurements", they are different representations of the same one.

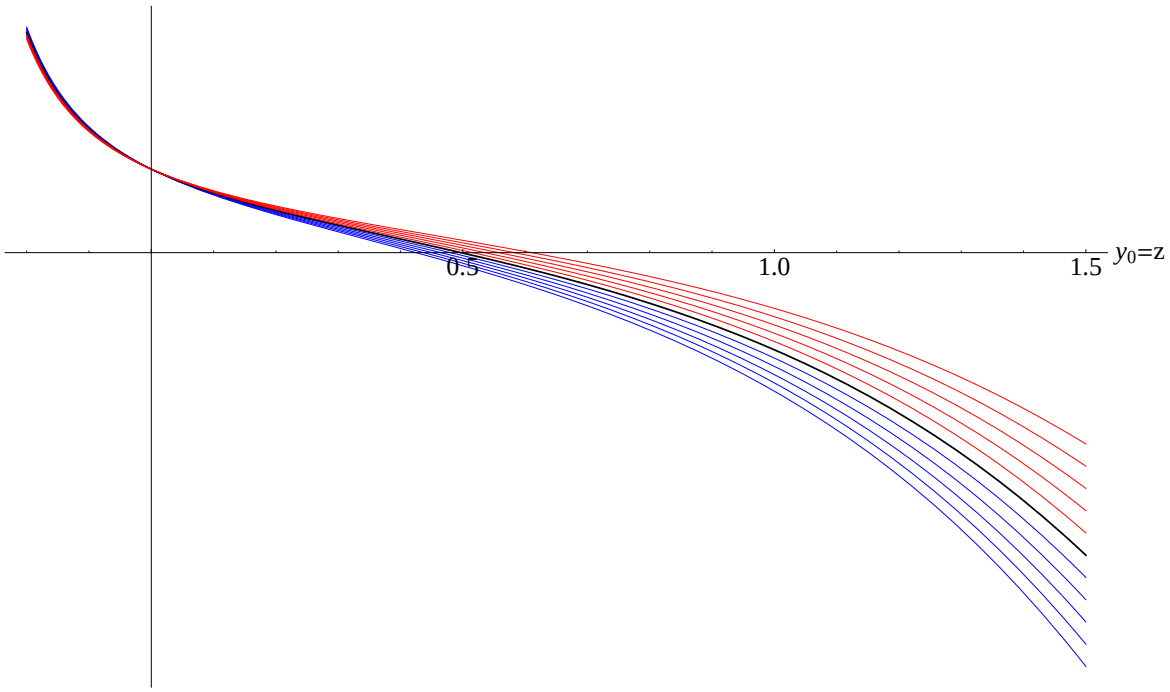

Figure 3.17. The average of the fifteen "natural" $\ddot{a}(z)$ functions from Figure 3.15, namely those in columns one, five and six, and rows two, four, six, seven and eight, extended to negative z, i.e. to the future. The color coding has the same meaning as in Figures 3.11-3.13. The horizontal axis shows $z = y_0$, ticked with intervals $\Delta z = 0.1$, and the vertical axis is in arbitrary units.

Consideration of these gives for the redshift of transition from deceleration in the past to current acceleration as

$$z_{\mathrm{t,flat}} = 0.50^{+0.08}_{-0.10} \tag{3.16}$$

for the case the universe is flat, and

$$z_{\mathrm{t},+} = 0.61^{+0.12}_{-0.13} \quad z_{\mathrm{t},-} = 0.42^{+0.08}_{-0.08} \tag{3.17}$$

for the most positively and most negatively curved universes considered.

In that figure, we also show an extension towards negative z, i.e the future – after all, the curves represent analytical functions– predicting that the acceleration will continue to increase. However, such prediction is risky because of the propensity of the fits to diverge when moving away from the range of the data; hence we kept the extension short –only up to $z = -0.2$; Still, while the extent of predicted increase of acceleration depends on the chosen family (parametrization) for $d_L(z)$, *some* increase is predicted for each one of the 15 choices, at least in this range, and for zero curvature.

Obviously we can extend the past acceleration to $z \sim 6$, where GRB data is relevant (Figure 3.18). However, due to the large error bars at those redshifts, this extension is not very informative.

3.3.3. Is the universe accelerating *now*?

In Figures 3.13 and 3.15, we see that as $z \to 0$, $\ddot{a}$ approaches the same value for all curvatures. This may seem surprising, since most of the studies of the expansion history of the universe start from a physical model, therefore posit a dependence between the present value of acceleration and spatial curvature. Then, one would need complementary and independent data on the curvature of the universe (e.g. from the power spectrum of the CMB temperature anisotropies; a detailed discussion on the degeneracy between deceleration parameter and spatial curvature for various models

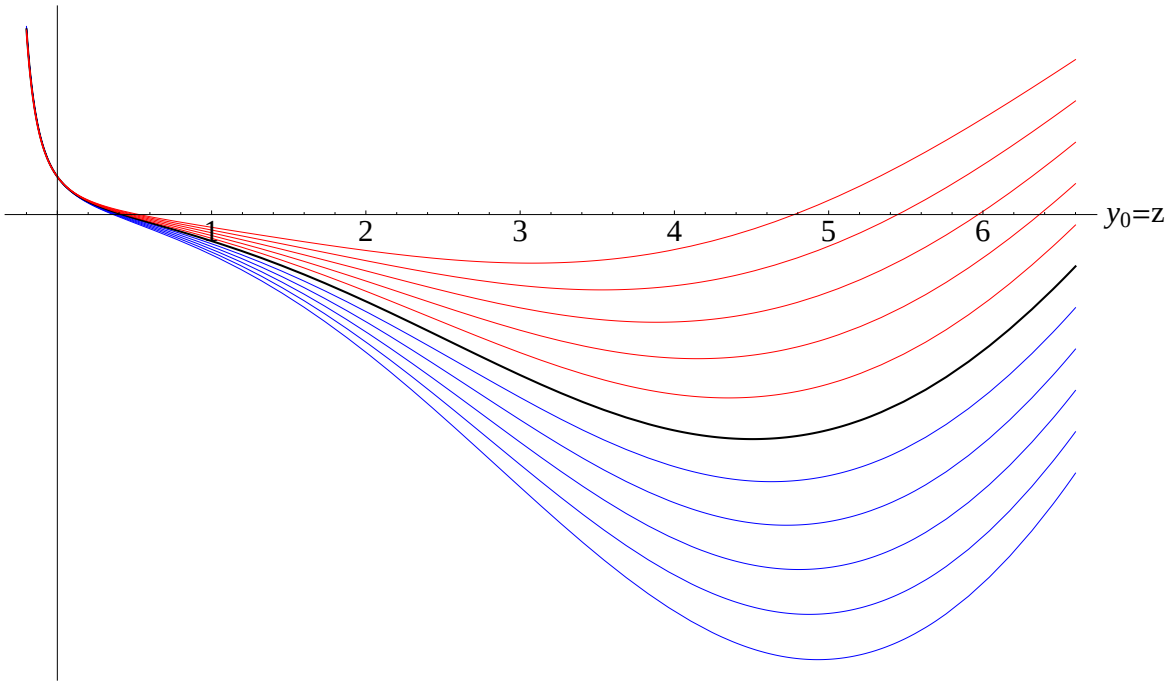

Figure 3.18. Acceleration history for the whole range including GRB data, plotted for function family F7 and redshift variable $y5$.

can be found in [27]). However, $\dot{A}(t)$ (where A is a shorthand for a/a_0) can be measured without any assumptions about curvature, and in principle, so can $\ddot{A}$, simply by waiting. To show this explicitly, let us investigate the analytical relationship between $\ddot{A}_{\text{now}}$ and $d_L(z)$, which can be evaluated in terms of redshift, using (1.10):

$$\ddot{A} = \frac{2}{(1+z)^3}\dot{z}^2 - \frac{1}{(1+z)^2}\ddot{z} \tag{3.18}$$

where $\dot{z}$ can be plugged in from (3.3),

$$\dot{z} = \frac{-c(1+z)\sqrt{1-\kappa\frac{d_L^2}{(1+z)^2}}}{\frac{d}{dz}\left[\frac{d_L}{1+z}\right]} = f(z)\sqrt{1-\kappa D^2(z)} \tag{3.19}$$

where $D(z) = d_L(z)/(z+1)$, sometimes called "photon count distance" [3], and $f(z)$ is the part outside the square root. Now, acceleration takes the form

$$\ddot{A} = \frac{2}{(1+z)^3}\left(f(z)\sqrt{1-\kappa D^2(z)}\right)^2 - \frac{1}{(1+z)^2}\frac{d}{dt}\left(f(z)\sqrt{1-\kappa D^2(z)}\right) \tag{3.20}$$

For $z \to 0$ it is easy to show that $D(z) \to 0$. Recalling $(D^2)^{\cdot} = 2D\dot{D}$, we have

$$\ddot{A}_{\rm now} = \left(2f^2 - \dot{f}\right)_{\rm now} = \left(2f^2 - f'\dot{z}\right)_{\rm now} \tag{3.21}$$

where $(')$ denotes derivative with respect to z. Putting $\dot{z}$ in once more,

$$\ddot{A}_{\rm now} = \left(2f^2 - f'f\right)_{\rm now} \tag{3.22}$$

Finally replacing $f(z)$ and rearranging terms,

$$\ddot{A}_{\rm now} = \left(\frac{c^2}{d_L'^3}\left(d_L'' - d_L'\right)\right)_{\rm now} \tag{3.23}$$

Thus we have shown that the present acceleration is independent of spatial curvature for given $d_L(z)$, and can be evaluated from data without assuming any theory of gravity. Equivalently, the result (3.23) can be reached from the MacLaurin series for $d_L(z)$ for FRW background,

$$d_L(z) = \frac{c}{H_0}\left[z + \frac{1}{2}(1 - q_0)z^2 + ...\right] \tag{3.24}$$

evaluating the first two derivatives at $z = 0$ (it turns out that k appears in the third term – see e.g. [28]).

3.4. Inferences in GR about the content of the universe

Up to this point we did not specify any theory of gravitation in our work. However it is appropriate now to assume General Relativity so that we can comment on the matter-energy content of the universe. First Einstein's equation in FRW framework gives

$$H^2 + \frac{kc^2}{a^2} = \frac{8\pi G}{3c^2}\rho \tag{3.25}$$

hence it is straightforward to construct $\rho(z)$ using (3.13). Using $u = z + 1$ as independent variable for future convenience, we plot an example for the evolution of matter-energy density, for different spatial curvatures in Figure 3.19. This particular figure was created using redshift variable $y5$ and fit family F7.

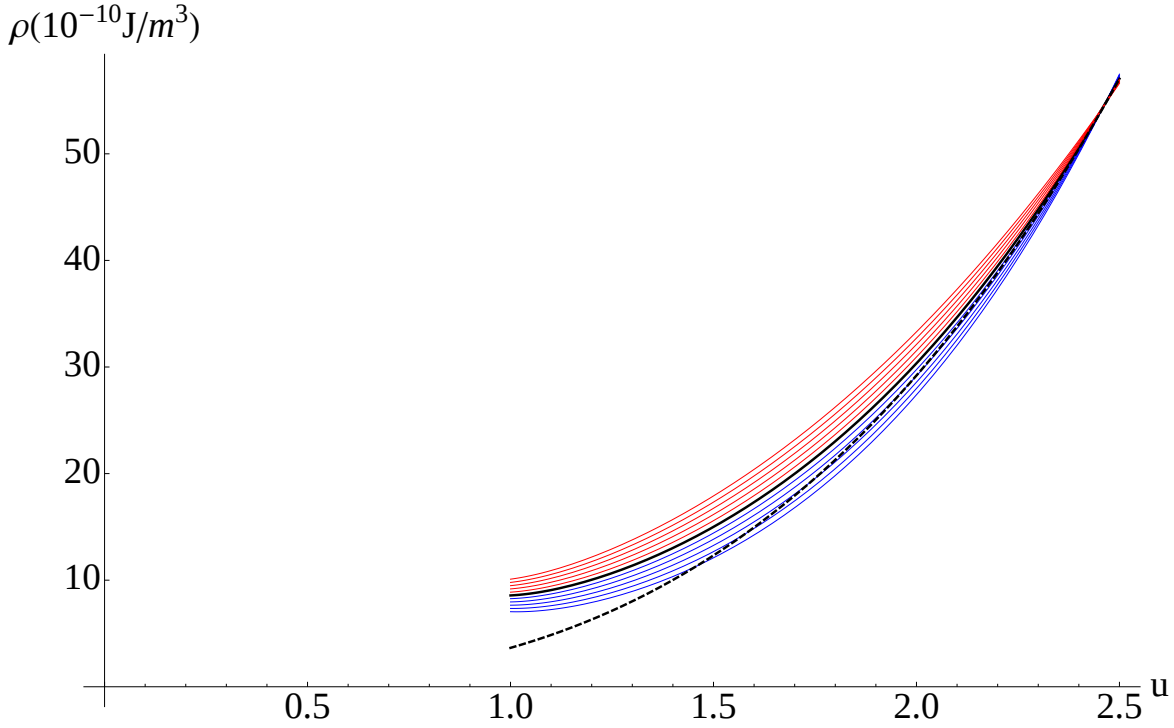

Figure 3.19. The density of the universe as function of $u = z + 1$, as calculated using the redshift variable $y5$ and fit family F7, assuming Einstein gravity. The color-coding is the same as used in Figure 3.12. Note the intersection around $z \approx 1.5$. The dashed curve shows matter density, passing through the intersection point.

An interesting feature manifests itself in this figure; there is an intersection point at $z \sim 1.5$ for curves with different spatial curvatures. To check the existence of this point analytically we plug (3.3) in (3.25) and get

$$\rho(z) = \frac{3c^2}{8\pi G}\left(c^2(1-\kappa D^2)\left(\frac{dD}{dz}\right)^{-2} + c^2\kappa(z+1)^2\right) \tag{3.26}$$

where $D(z)$ was defined in Subsection 3.3.3. This expression is linear in κ, hence for z values at which the coefficient of κ vanishes, the density *will* be independent of

curvature *for given* $d_L(z)$. The condition for this to be realized can be found as

$$D^2 = \left(\frac{dD}{dz}\right)^2 (z+1)^2 \tag{3.27}$$

which means that the slope of D, written as function of $u = z+1$, is equal to the slope of the chord connecting the point to the origin (note that both u and D are positive in the region of interest), it is not at all obvious that a solution will exist. The curvature-independence of density makes these points, –if and when they exist– special, and our analysis suggest that one such point exist for our universe; we call it z_*.

This point can be useful. For example, assuming that all contributions to the energy density of the universe are positive, it enables us to put an upper limit on the current value of matter density of our universe by equating (3.26) to the density of matter-dominated universe at $z = z_*$:

$$\frac{3c^4}{8\pi G}\left(\frac{dD}{dz}\right)^{-2}_{(z=z_*)} = \rho_{0\mathrm{m,max}}(z_*+1)^3 \tag{3.28}$$

where $\rho_{0\mathrm{m,max}}$ is the value of the dashed curve in Figure 3.19 at $u = 1$. Using Eq. 3.27 and the definition of $D(z)$,

$$\rho_{0\mathrm{m,max}} = \frac{3c^4}{8\pi G}\frac{z_*+1}{d_L^2(z_*)} \tag{3.29}$$

which can be converted into an upper bound for the density parameter for matter today, $\Omega_{0m,\mathrm{max}}$. The results for the 15 "natural" $d_L(z)$ functions referred to after Figure 3.15 are given in Table 3.4. It is worth noting that the newly introduced variable $y5$ gives remarkably more consistent values of z_*, hence $\Omega_{0m,\mathrm{max}}$.

For the total current density of the universe we have

$$\Omega_0 = 1 + \frac{kc^2}{H_0^2 a_0^2} = 1 + k'\kappa_0 \frac{c^2}{H_0^2} \approx 1 + 0.18k' \tag{3.30}$$

where the first equality easily follows from (3.25), and the others from our definitions of κ_0 and k'. Since the density of radiation is negligible in the recent universe, the gap between these Ω_0 values and the numbers in Table 3.4 point to the existence of something else in the universe, the lower limit on whose current density is

$$\Omega_{0,\mathrm{de}} \geq 0.28 \tag{3.31}$$

In principle, it is also possible to put upper limits on radiation energy density of the universe in a similar manner. However these limits will be about four orders of magnitude higher than the energy density of the cosmic background radiation, so they cannot meaningfully limit the number of relativistic species filling the universe.

Table 3.4. z_* and $\Omega_{0m,\mathrm{max}}$ with their estimated errors calculated for 15 different $d_L(z)$ functions and assuming Einstein gravity.

$d_L(z)$	z_*	$\Omega_{0m,\mathrm{max}}$
y0-F2	$1.34^{+0.04}_{-0.03}$	$0.502^{+0.035}_{-0.040}$
y0-F4	$1.35^{+0.05}_{-0.03}$	$0.498^{+0.038}_{-0.047}$
y0-F6	$1.38^{+0.05}_{-0.04}$	$0.475^{+0.040}_{-0.042}$
y0-F7	$1.47^{+0.08}_{-0.06}$	$0.421^{+0.046}_{-0.054}$
y0-F8	$1.43^{+0.07}_{-0.05}$	$0.444^{+0.043}_{-0.049}$
y5-F2	$1.44^{+0.08}_{-0.05}$	$0.438^{+0.044}_{-0.054}$
y5-F4	$1.46^{+0.09}_{-0.06}$	$0.426^{+0.046}_{-0.054}$
y5-F6	$1.46^{+0.08}_{-0.06}$	$0.425^{+0.047}_{-0.051}$
y5-F7	$1.46^{+0.09}_{-0.06}$	$0.428^{+0.045}_{-0.054}$
y5-F8	$1.43^{+0.07}_{-0.05}$	$0.441^{+0.041}_{-0.047}$
y6-F2	$1.34^{+0.04}_{-0.03}$	$0.502^{+0.036}_{-0.040}$
y6-F4	$1.36^{+0.04}_{-0.04}$	$0.491^{+0.044}_{-0.041}$
y6-F6	$1.38^{+0.05}_{-0.04}$	$0.475^{+0.040}_{-0.042}$
y6-F7	$1.47^{+0.08}_{-0.06}$	$0.421^{+0.046}_{-0.050}$
y6-F8	$1.43^{+0.07}_{-0.05}$	$0.444^{+0.043}_{-0.049}$

Considering the possibility of very large number of (sterile) massless particle species will give a smaller upper limit on the current density of matter+radiation, hence a larger lower limit on the density of *dark energy*. Hence we quote (3.31) as our result.

We can also use the second Einstein's equation which will give effective pressure $p(z)$ of the content of the Universe. Dividing it by the energy density we get $w(z) = p/\rho$; the effective equation of state parameter for the Universe (Figure 3.20).

Again we see an intersection point similar to the one in Figure 3.19. With hindsight, we can mathematically predict this point too, but it does not seem to have any physical significance. We find the current value of w to be between -0.7 and -0.9 depending on the assumption for curvature, with an estimated error of 0.015. It should be noted that this is the total EoS parameter, not the w of dark energy, which is reported in recent literature [12, 16] with a central value less than -1; the two statements are not inconsistent. An extrapolation towards the future shows a trend toward

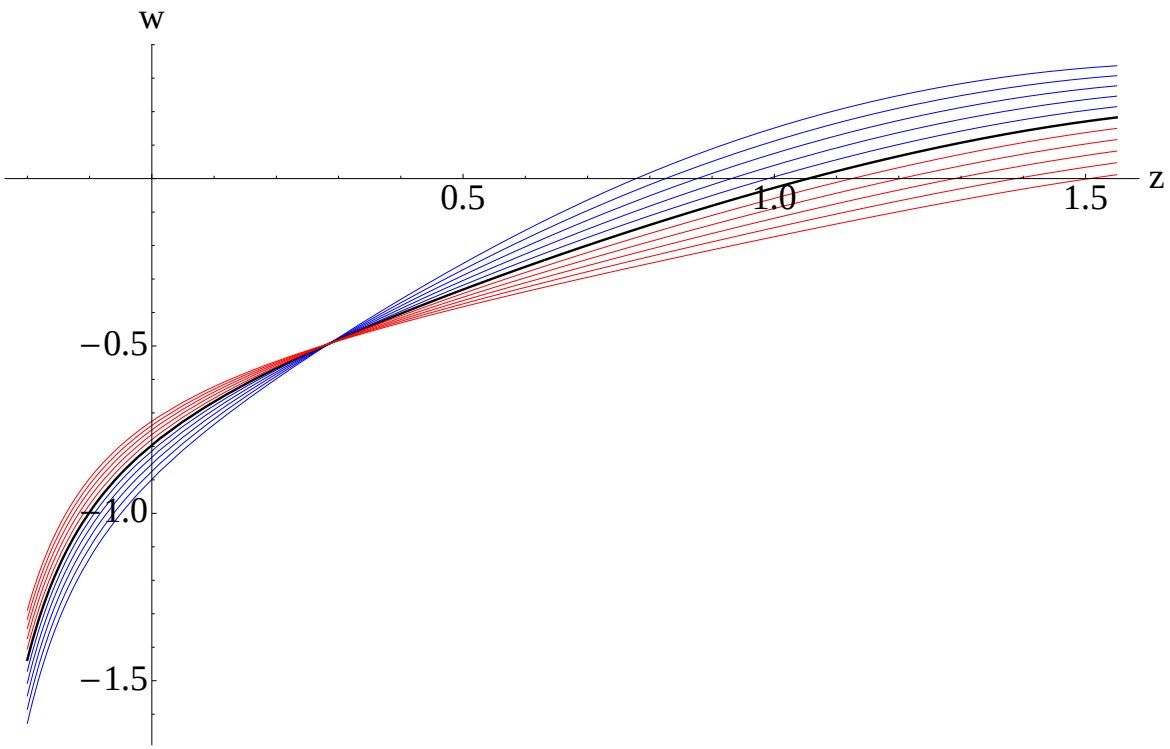

Figure 3.20. The average $w(z)$, in the framework of Einstein gravity, found from the fifteen functions we used in Figure 3.17, extended to negative z, i.e. to the future. The color coding has the same meaning as in Figures 3.11-3.13.

phantom-domination. However, for same reasons as Figure 3.17, the prediction is not very reliable, in fact, in this case, there are choices (3 out of 15) of $d_L(z)$ for which w does not decrease; so again the extrapolation is kept short.

4. IDEAS ON THE EXPANSION OF THE UNIVERSE

4.1. Modelling the expansion between two regimes

One interesting pursuit might be to reconstruct expansion characteristics of the universe between radiation and matter dominated eras more accurately modelling with one relativistic massive fluid. To do so we may start with the kinetic theory for relativistic gases which leads to the pressure expression as follows:

$$p = \frac{Nmc^2}{3V}\left(\overline{\gamma} - \overline{1/\gamma}\right) \tag{4.1}$$

where γ is the standard special relativistic speed factor, m the mass of the particles consisting the fluid, N the number of particles and V the volume in which the fluid is contained. Here $\overline{\gamma}$ and $\overline{1/\gamma}$ can be calculated using Maxwell-Jüttner distribution:

$$f(\gamma) = \frac{\gamma^2\beta}{\theta K_2(1/\theta)} \exp\left(-\gamma/\theta\right) \tag{4.2}$$

where $\beta = v/c = \sqrt{1 - 1/\gamma^2}$, $\theta = k_B T/mc^2$ and K_α is modified Bessel function of the second kind of order α. This distribution is a relativistic generalisation to Maxwell-Boltzman but it lacks quantum features unlike Fermi-Dirac or Bose-Einstein distributions. Nevertheless it suits our purposes in this calculation.

We get

$$\overline{\gamma} = \frac{K_1(1/\theta) + 3\theta K_2(1/\theta)}{K_2(1/\theta)} \tag{4.3}$$

and

$$\overline{1/\gamma} = \frac{K_1(1/\theta)}{K_2(1/\theta)} \tag{4.4}$$

Once we know p and ρ we can write down deceleration parameter q using Einstein's equations for a flat universe, which turns out to be:

$$q(1/\theta) = 1 - \frac{K_1(1/\theta)}{2K_1(1/\theta) + 6\theta K_2(1/\theta)} \tag{4.5}$$

This part of the calculations are consistent with the earlier work [29]. Equation 4.5 is an exact expression for the deceleration parameter as a function of temperature between radiation and matter dominated eras (Figure 4.1).

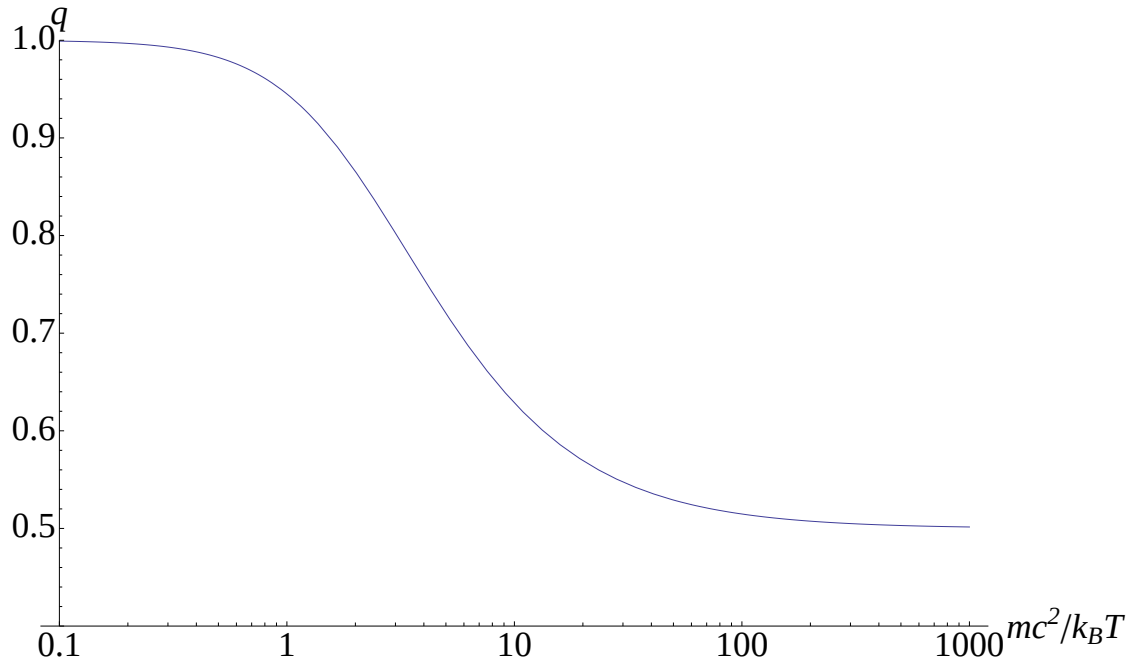

Figure 4.1. Evolution of deceleration parameter between radiation and matter dominated eras. Horizontal axis shows $1/\theta = mc^2/k_BT$.

It may be interesting to turn this expression into an ansatz which may be applied between any two regimes:

$$q(1/\theta) = q_i - (q_i - q_f)\frac{K_1(\theta_i/\theta)}{K_1(\theta_i/\theta) + 3\theta/\theta_i K_2(\theta_i/\theta)} \tag{4.6}$$

where q_i and q_f are the deceleration values for the initial and final states respectively and θ_i is the initial energy level.

For example, for the interpolation between matter and Λ dominated eras the parameters q_i and q_f should be 0.5 and -1 respectevily. This is actually again a single fluid model in which dark matter is *cooling down* to Λ (Figure 4.2). Such interacting dark sector models are investigated heavily in literature [30].

One can easily see that $k_B T_i$, the energy level at which *dark decay* is triggered, is a free parameter of the model but it can be estimated through observations. If we

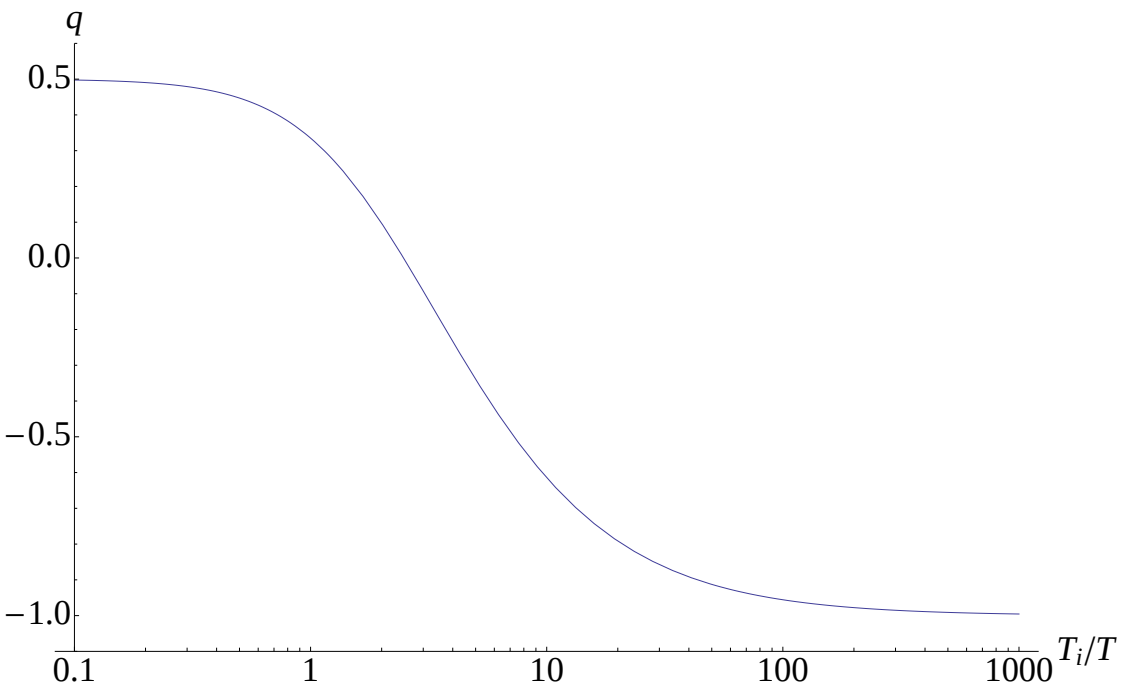

Figure 4.2. Evolution of deceleration parameter between matter and Λ dominated eras.

assume that this ansatz describes our universe correctly, we can adopt the value of q_0 from expansion data and $\theta_0 = k_B T_0/mc^2$ from CMB anisotropy. For example, for $q_0 = -0.5$ and $T_0 = 2.73$ K estimated energy scale is $k_B T_i = 1.7 \times 10^{-3}$ eV.

4.2. Massive photons and modifications on observations

Observing an accelerated expansion is actually observing supernova fainter than expected. At the beginning there were concerns that this reduction may be due to absorption or scattering of light by intergalactic material rather than an accelerated expansion. One such popular suggestion was *gray dust*, an intergalactic medium which reduces the luminosity of distant objects but does not alter their *color* (therefore *gray*) [4]. This idea is however put to rest by more distant observations [31], since they reported larger apparent luminosities than the values predicted for the absorption or scattering of light by an intergalactic medium. In other words, it can be assumed that they are coming from a matter dominated, hence decelerating, era.

In a similar manner we wish to examine a scenario in which photons have mass and we should have a correction in our measurement. In this scenario, like any other massive particle, photons do not experience a redshift but a *momentum drag*. Luminosity is energy per unit time and classically it is reduced by $(1+z)^2$, both photon energy and inverse time are redshifted. But if the photons have mass, considering the detector-photon interaction only the reduction in kinetic energies should be relevant. So we may rewrite the expression for luminosity distance in an expanding universe as,

$$d_L^2(z) = a_0^2 r^2 (1+z) \left(\frac{K_0}{K}\right) \tag{4.7}$$

where K denotes the kinetic energy of photons. Reduction in kinetic energy can be written as,

$$\frac{K_0}{K} = \frac{\sqrt{\hbar^2 k_0^2 c^2 + m^2 c^4} - mc^2}{\sqrt{\hbar^2 k^2 c^2 + m^2 c^4} - mc^2} \tag{4.8}$$

where m is the photon mass and k is the wave number. Expanding space imposes that $k_0/k = (1+z)$ so,

$$\frac{K_0}{K} = \frac{\sqrt{(1+z)^2 + \tilde{\lambda}^2} - \tilde{\lambda}}{\sqrt{1+\tilde{\lambda}^2} - \tilde{\lambda}} \tag{4.9}$$

where $\tilde{\lambda} = \frac{mc\lambda}{h}$. With the assumption of a matter dominated flat universe, Equation 4.7 gives,

$$d_L(z) = 2\frac{c}{H_0}(\sqrt{1+z})\sqrt{\frac{\sqrt{(1+z)^2 + \tilde{\lambda}^2} - \tilde{\lambda}}{\sqrt{1+\tilde{\lambda}^2} - \tilde{\lambda}}} \tag{4.10}$$

a dispersion relation for luminosity distance. Through a simple fit for a sample wavelength $\lambda = 550 \times 10^{-9}$nm we can estimate photon mass $m \simeq 4.43$ eV (Figure 4.3). Of course, such an energy scale is robustly excluded. However, our estimation was made using general relativity. For theories predicting a photon mass [32] our calculation needs to be rethought to see if there is any nonnegligible correction to the photon energies detected.

4.3. Foam-like structure and its cosmological implications

A major criticism of ΛCDM is the *coincidence problem*. To summarise, we live in a time at which $\Omega_{\rm M}$ and Ω_Λ are comparable; transition between the matter and Λ dominated eras is just taking place and compared to the lifetimes of these eras this transition time is extremely short, thus we are living in a very special period in the

history of the universe [33].

Every low probability event like this may raise the question "why now?" yet one can always give the somewhat anthropic answer "why not?". Nevertheless, this coincidence, which can be interpreted as an initial fine-tuning problem also, let the researchers look for dark energy models that are triggered at some point near in time, so-called tracker solutions [34]. It is also natural to link accelerated expansion, a recent phenomenon, to another recent global occurrence in the universe, large scale structure formation. The growth in nonlinearity in matter densities in the recent past occasionally comes as an inspiration for observed acceleration. Most of the studies point out that we may be living in a big void and universe might appear *as if* accelerating to us [35].

We want to take a different approach. Inspired by the web-like structure revealed by the galaxy redshift observations and the computer simulations, we replace the homogeneous and isotropic equation of state with a statistically homogeneous and statistically isotropic one. Such an equation of state is confirmed for dry foam (bubbles

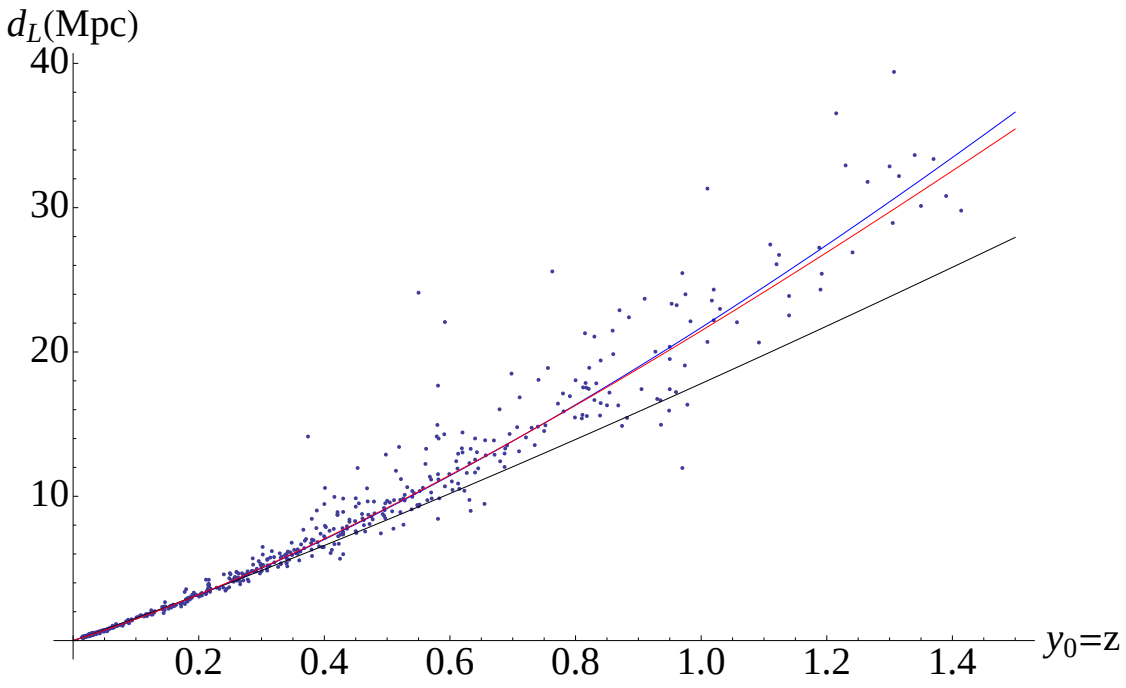

Figure 4.3. Massive photon cosmology (blue) with ΛCDM (red) and matter dominated model (black) compared to Union 2.1 data.

with ideal gas in them) in fluid mechanics [36],

$$p_{\text{ext}}V + \frac{2}{3}\sigma A = NT \tag{4.11}$$

Here p_{ext} is the total pressure of the system, σ is the surface tension, A is the total area of the interfaces between bubbles, N is the number of ideal gas particles and T is the temperature. If we incorporate this model to cosmology, the assumption is that almost all the matter is concentrated in thin walls of structure and of course $T = 0$. So, it is possible to come up with a negative pressure term in the form of tension in structure walls,

$$p = -\frac{2}{3}\frac{\sigma A}{V} \tag{4.12}$$

The term $\frac{\sigma A}{V}$ is the surface energy per volume and will be denoted by ρ_s from now on.

Deceleration parameter q from Einstein's equations in a flat space is

$$q = \frac{1}{2}\left(1 + 3\frac{p}{\rho_c}\right) \tag{4.13}$$

If we plug (4.12) to the above we get,

$$q = \frac{1}{2}\left(1 - 2\frac{\rho_s}{\rho_c}\right) \tag{4.14}$$

One can easily see that if $\rho_s = \rho_c$ for which all the energy density in the universe is in the form of surface energy, we recover $q = -\frac{1}{2}$, the value for a universe dominated by cosmic domain walls.

If we move on without introducing any exotic component like dark energy or cosmic walls it is convenient to interpret this tension energy as Newtonian gravitational potential within dark matter structure. Assuming that we have sheets of uniform mass density we can make the following estimation,

$$\rho_s = \frac{U}{V} \sim G\sigma_s^2 \tag{4.15}$$

where U is the gravitational potential energy and σ_s is the surface mass density. We assume that the voids are almost empty, so

$$\sigma_s c^2 = \rho_c \frac{V}{A} \tag{4.16}$$

The important parameter is V/A, the typical volume-to-surface area ratio of a cosmic spherical void. In terms of void radius R this ratio is given by $R/3$. Rearranging terms we get the following equation,

$$q = \frac{1}{2}\left(1 - \frac{H^2 R^2}{12\pi c^2}\right) \tag{4.17}$$

Let us calculate the term with the negative sign to see if it can sustain any acceleration. The Hubble parameter today can be roughly estimated as $H \sim 70$ km/s/Mpc and the average void size estimated from surveys is $R \sim 100$ Mpc. It turns out to be that introduced contribution is about 10^{-6}. We can also calculate the necessary void size for acceleration (e. g. $q = -1/2$) which turns out to be $R \sim 10^5$ Mpc, much bigger than the supervoids suggested in literature.

Does this mean the end of this assertion? One possible way out may be introducing a DM-DM interaction, a "fifth force" as named in literature [30], much stronger than gravity, which will eventually increase surface energy. But a long-range force this strong is likely to break the structure formation process, so this alternative is to be considered with high caution. Alternatively, it may be argued that there lies a dark matter infrastructure with voids big enough to accommodate acceleration and is inaccessible to our observations yet. Again, this idea needs to be well-thought since it may introduce a whole new scenario for structure formation.

5. CONCLUSION

In our analysis in chapter 3, we have fit various functions to the cosmological luminosity distance data, mostly the Union 2.1 Type Ia supernovae, and tried to extract information about the expansion history of the universe. The ansätze used for the luminosity distance function $d_L(z)$ were motivated not by any physical model, but by facilitation of the operations for going from the function $d_L(z)$ to the function $a(t)$, the scale factor of the universe. We first took the number of parameters in the $d_L(z)$ ansätze variable, forming families, and for each family we took the member with the minimum χ^2/d.o.f. We also tried a number of different redshift variables.

Since in most of the work we did not use any law of gravity, our work is *model-independent*; in other words, we are simply studying the geometry of the universe, i.e. doing *cosmography*.

We found that in some models it does not make sense to try to extract more than two cosmological parameters, although this number is more often three or four, up to six in some models. We found that Padé approximants and expressions involving $(z+1)$ as a factor give slightly better fits to $d_L(z)$ data than polynomials of the redshift variables, possibly multiplied by linear or quadratic exponentials of the same. We also saw that y_5, the redshift parameter we introduced, gives better fits than the other redshift parameters in the literature. Yet we found that no model fits significantly better than ΛCDM.

We demonstrated that *for "measured" $d_L(z)$ function*, the current acceleration of the universe does not depend on its curvature (a known result, but not widely appreciated in this context). But we found that the supernova data are too scattered and have too large errors to *by themselves* show a transition from deceleration to acceleration in the past of the universe, at least not for the ansätze we used. We decided that the procedural problem lies in the convergence properties of polynomials, which form components of the ansätze; and decided that it is possible to tame these

divergences by including GRB data which reach out to much higher redshifts. Even though they are not really model-independent, we argue that due to their comparatively small number and large uncertainties, the work will not be contaminated much with physical models, while still serving to tame the dominance of higher order powers in polynomials. With their inclusion, we found the deceleration-acceleration transition at redshift $z_{\mathrm{t,flat}} = 0.50^{+0.08}_{-0.10}$ for a flat universe, larger (earlier) for positive spatial curvature, and smaller (later) for negative.

Finally assuming Einstein gravity, we found that there is a special redshift value, call it z_*, at which the density of the universe is independent of its curvature, again *for "measured" $d_L(z)$ function*. This enables us to put an upper limit of roughly 0.50 ± 0.04 on the current density parameter of matter, dark or not, *without using an EoS for the cosmic fluid*. This translates into a lower limit for current *dark energy* density parameter of roughly 0.3, assuming the "worst" case for the curvature of the universe.

We can also find the total EoS parameter $w(z)$ for the universe; we find that the EoS is not yet *phantom*, but it seems to be evolving in that direction. Of course, assuming an alternative theory of gravitation would bring (possibly qualitatively) different interpretations than in these last two paragraphs.

As a remark we would like to address an interesting discussion on cosmography in [37]. A definition of *the ideal cosmography* is given as "determining the coefficients of an arbitrary metric describing the universe with perfect observations without the use of field equations" and it is shown that the task is impossible; at least one of the metric coefficients remains coupled to the energy density. In our analysis we have shown that it is possible, at least numerically, to find $a(t)$ from practical data. So, the other parameter in our specific metric, k/a_0^2, remains to be determined with assumptions on cosmological model, which leads us back to one of our arguments at the introduction. An example of a non-zero curvature cosmological model explaining CMB anisotropy perfectly may be found in [38].

In chapter 4, we have investigated three new ideas on the expansion history of the universe. First we modelled the era between radiation and matter dominations with a cooling relativistic fluid and extended our result as an ansatz for the recent universe where dark matter decays into dark energy. We estimated an energy level for DM-DE interaction to start. Then we looked for the effects of massive photons on observations. We concluded that for the measured luminosity distances to mimic an accelerated expansion mass of the photons need to be much larger than upper bounds put by experiments. Lastly we investigated the effect of inhomogeneities in the matter density on the expansion. We introduced an equation of state that takes the tension in the cosmic structure into account and we showed that for only enormously large voids accelerated expansion can be achieved.

The next big survey in observational cosmology is the Dark Energy Survey (DES) [39]. It is a wide field camera in Chile, which started operating in 2012 and it is expected to generate a catalog of 3×10^8 galaxies and thousands of SNe Ia. The first cosmological results are expected to come in the following years. For the space based observations, the next step will be the Euclid satellite, a proposed mission by ESA to be launched in the next decade. The projection is to observe $\sim 10^8$ galaxies around redshift $z\sim 2$. In the meantime SDSS-IV mission is going to carry the flag of galaxy surveys.

The coming decades should bring an increase in the number of the SNe Ia observations. If technology improves such that the uncertainties of the luminosity measurements decrease, it should be possible to find better fits; however, the scatter should also decrease for those fits to make more sense and the reconstruction of the scale factor function and other inferences made in this work to be more reliable. There is recent work [40, 41] suggesting that Type Ia supernovae might not be all identical after all, a potential development reminiscent of the discovery of the different types of Cepheids in 1940's. If confirmed, this would also lead to a reevaluation of existing data, possibly decreasing scatter, and together with the new data, might lead to the required improvement.

REFERENCES

1. Hubble, E., "A Relation between Distance and Radial Velocity among Extra-Galactic Nebulae", *Proceedings of the National Academy of Science*, Vol. 15, pp. 168–173, Mar. 1929.

2. Rapetti, D., S. W. Allen, M. A. Amin and R. D. Blandford, "A kinematical approach to dark energy studies", *Monthly Notices of the Royal Astronomical Society*, Vol. 375, No. 4, pp. 1510–1520, 2007.

3. Cattoën, C. and M. Visser, "Cosmography: Extracting the Hubble series from the supernova data", *arXiv preprint arXiv:gr-qc/0703122*, 2007.

4. Weinberg, S., *Cosmology*, Oxford Univ. Press, 2008.

5. Hu, W. and S. Dodelson, "Cosmic microwave background anisotropies", *Rev. Astron. Ap*, Vol. 40, p. 171, 2002.

6. Montanari, F. and R. Durrer, "New method for the Alcock-Paczyński test", *Physical Review D*, Vol. 86, No. 6, p. 063503, 2012.

7. Abbott, B., R. Abbott, T. Abbott, M. Abernathy, F. Acernese, K. Ackley, C. Adams, T. Adams, P. Addesso, R. Adhikari *et al.*, "Observation of Gravitational Waves from a Binary Black Hole Merger", *Physical Review Letters*, Vol. 116, No. 6, p. 061102, 2016.

8. Fields, B. D., "The primordial lithium problem", *arXiv preprint arXiv:1203.3551*, 2012.

9. Kashlinsky, A., F. Atrio-Barandela, D. Kocevski and H. Ebeling, "A measurement of large-scale peculiar velocities of clusters of galaxies: results and cosmological implications", *The Astrophysical Journal Letters*, Vol. 686, No. 2, p. L49, 2008.

10. Riess, A. G., A. V. Filippenko, P. Challis, A. Clocchiatti, A. Diercks, P. M. Garnavich, R. L. Gilliland, C. J. Hogan, S. Jha, R. P. Kirshner *et al.*, "Observational evidence from supernovae for an accelerating universe and a cosmological constant", *The Astronomical Journal*, Vol. 116, No. 3, p. 1009, 1998.

11. Perlmutter, S., G. Aldering, G. Goldhaber, R. Knop, P. Nugent, P. Castro, S. Deustua, S. Fabbro, A. Goobar, D. Groom *et al.*, "Measurements of Ω and Λ from 42 high-redshift supernovae", *The Astrophysical Journal*, Vol. 517, No. 2, p. 565, 1999.

12. Suzuki, N., D. Rubin, C. Lidman, G. Aldering, R. Amanullah, K. Barbary, L. Barrientos, J. Botyanszki, M. Brodwin, N. Connolly *et al.*, "The Hubble Space Telescope Cluster Supernova Survey. V. Improving the dark-energy constraints above z>1 and building an early-type-hosted supernova sample", *The Astrophysical Journal*, Vol. 746, No. 1, p. 85, 2012.

13. Schaefer, B. E., "The Hubble diagram to redshift>6 from 69 gamma-ray bursts", *The Astrophysical Journal*, Vol. 660, No. 1, p. 16, 2007.

14. Melia, F., "The high-z quasar Hubble Diagram", *Journal of Cosmology and Astroparticle Physics*, Vol. 2014, No. 01, p. 027, 2014.

15. Ade, P. A. R., N. Aghanim, M. Arnaud, M. Ashdown, J. Aumont, C. Baccigalupi, A. J. Banday, R. B. Barreiro, J. G. Bartlett and et al., "Planck 2015 results. XIII. Cosmological parameters", *arXiv preprint arXiv:1502.01589*, 2015.

16. Ade, P., N. Aghanim, C. Armitage-Caplan, M. Arnaud, M. Ashdown, F. Atrio-Barandela, J. Aumont, C. Baccigalupi, A. J. Banday, R. Barreiro *et al.*, "Planck 2013 results. XVI. Cosmological parameters", *Astronomy & Astrophysics*, Vol. 571, p. A16, 2014.

17. Anderson, L., É. Aubourg, S. Bailey, F. Beutler, V. Bhardwaj, M. Blanton, A. S. Bolton, J. Brinkmann, J. R. Brownstein, A. Burden *et al.*, "The clustering of

galaxies in the SDSS-III Baryon Oscillation Spectroscopic Survey: baryon acoustic oscillations in the Data Releases 10 and 11 Galaxy samples", *Monthly Notices of the Royal Astronomical Society*, Vol. 441, No. 1, pp. 24–62, 2014.

18. Busca, N. G., T. Delubac, J. Rich, S. Bailey, A. Font-Ribera, D. Kirkby, J.-M. Le Goff, M. Pieri, A. Slosar, É. Aubourg, J. Bautista *et al.*, "Baryon acoustic oscillations in the Lyα forest of BOSS quasars", *Astronomy & Astrophysics*, Vol. 552, p. A96, 2013.

19. Semiz, İ. and A. K. Çamlıbel, "What do the cosmological supernova data really tell us?", *Journal of Cosmology and Astroparticle Physics*, Vol. 2015, No. 12, p. 038, 2015.

20. Aviles, A., C. Gruber, O. Luongo and H. Quevedo, "Cosmography and constraints on the equation of state of the Universe in various parametrizations", *Physical Review D*, Vol. 86, No. 12, p. 123516, 2012.

21. Sutherland, W. and P. Rothnie, "On the luminosity distance and the epoch of acceleration", *Monthly Notices of the Royal Astronomical Society*, Vol. 446, No. 4, pp. 3863–3873, 2015.

22. Gruber, C. and O. Luongo, "Cosmographic analysis of the equation of state of the universe through Padé approximations", *Physical Review D*, Vol. 89, No. 10, p. 103506, 2014.

23. Aviles, A., A. Bravetti, S. Capozziello and O. Luongo, "Precision cosmology with Padé rational approximations: Theoretical predictions versus observational limits", *Physical Review D*, Vol. 90, No. 4, p. 043531, 2014.

24. Wei, H., X.-P. Yan and Y.-N. Zhou, "Cosmological applications of Padé approximant", *Journal of Cosmology and Astroparticle Physics*, Vol. 2014, No. 01, p. 045, 2014.

25. Riess, A. G., L.-G. Strolger, J. Tonry, S. Casertano, H. C. Ferguson, B. Mobasher, P. Challis, A. V. Filippenko, S. Jha, W. Li *et al.*, "Type Ia supernova discoveries at z>1 from the Hubble Space Telescope: Evidence for past deceleration and constraints on dark energy evolution", *The Astrophysical Journal*, Vol. 607, No. 2, p. 665, 2004.

26. Semiz, I., "Approximations for the natural logarithm from solenoid-toroid correspondence", *arXiv preprint arXiv:1503.03830*, 2015.

27. Mörtsell, E. and C. Clarkson, "Model independent constraints on the cosmological expansion rate", *Journal of Cosmology and Astroparticle Physics*, Vol. 2009, No. 01, p. 044, 2009.

28. Visser, M., "Jerk, snap and the cosmological equation of state", *Classical and Quantum Gravity*, Vol. 21, No. 11, pp. 2603–2615, 2004.

29. Szekeres, P. and A. S. Barnes, "Cosmologies with a Synge gas and radiation", *Monthly Notices of the Royal Astronomical Society*, Vol. 189, No. 4, pp. 767–775, 1979.

30. Bolotin, Y. L., A. Kostenko, O. A. Lemets and D. A. Yerokhin, "Cosmological evolution with interaction between dark energy and dark matter", *International Journal of Modern Physics D*, Vol. 24, No. 03, p. 1530007, 2015.

31. Riess, A. G., P. E. Nugent, R. L. Gilliland, B. P. Schmidt, J. Tonry, M. Dickinson, R. I. Thompson, T. Budavari, S. Casertano, A. S. Evans *et al.*, "The Farthest Known Supernova: Support for an Accelerating Universe and a Glimpse of the Epoch of DecelerationBased on observations with the NASA/ESA Hubble Space Telescope, obtained at the Space Telescope Science Institute, which is operated by AURA, Inc., under NASA contract NAS 5-26555.", *The Astrophysical Journal*, Vol. 560, No. 1, p. 49, 2001.

32. Akarsu, Ö., M. Arık, N. Katırcı and M. Kavuk, "Accelerated expansion of the universe à la the Stueckelberg mechanism", *Journal of Cosmology and Astroparticle Physics*, Vol. 2014, No. 07, p. 009, 2014.

33. Velten, H., R. vom Marttens and W. Zimdahl, "Aspects of the cosmological "coincidence problem"", *The European Physical Journal C*, Vol. 74, No. 11, pp. 1–8, 2014.

34. Steinhardt, P. J., L. Wang and I. Zlatev, "Cosmological tracking solutions", *Physical Review D*, Vol. 59, No. 12, p. 123504, 1999.

35. Räsänen, S., "Cosmological acceleration from structure formation", *International Journal of Modern Physics D*, Vol. 15, No. 12, pp. 2141–2146, 2006.

36. Aref, H. and D. L. Vainchtein, "The equation of state of a foam", *Physics of Fluids (1994-present)*, Vol. 12, No. 1, pp. 23–28, 2000.

37. Ellis, G. F., R. Maartens and M. A. MacCallum, *Relativistic cosmology*, Cambridge University Press, 2012.

38. Okouma, P. M., Y. Fantaye and B. A. Bassett, "How flat is our Universe really?", *Physics Letters B*, Vol. 719, No. 1, pp. 1–4, 2013.

39. Abbott, T., F. Abdalla, S. Allam, J. Aleksic, A. Amara, D. Bacon, E. Balbinot, M. Banerji, K. Bechtol, A. Benoit-Levy *et al.*, "The Dark Energy Survey: more than dark energy-an overview", *arXiv preprint arXiv:1601.00329*, 2016.

40. Milne, P. A., R. J. Foley, P. J. Brown and G. Narayan, "The changing fractions of type Ia supernova NUV–Optical subclasses with redshift", *The Astrophysical Journal*, Vol. 803, No. 1, p. 20, 2015.

41. Brown, P. J., E. Baron, P. Milne, P. W. Roming and L. Wang, "Theoretical clues to the ultraviolet diversity of type Ia supernovae", *arXiv preprint arXiv:1504.05237*, 2015.